8-2013

Transparent Antennas for Solar Cell Integration

Tursunjan Yasin
Utah State University

TRANSPARENT ANTENNAS FOR SOLAR CELL INTEGRATION

by

Tursunjan Yasin

A dissertation submitted in partial fulfillment
of the requirements for the degree

of

DOCTOR OF PHILOSOPHY

in

Electrical Engineering

Approved:

Dr. Reyhan Baktur Major Professor	Dr. Bedri A. Cetiner Committee Member
Dr. Edmund A. Spencer Committee Member	Dr. Jacob Gunther Committee Member
Dr. Bela G. Fejer Committee Member	Dr. Mark R. McLellan Vice President for Research and Dean of the School of Graduate Studies

UTAH STATE UNIVERSITY
Logan, Utah

2013

Abstract

Transparent Antennas for Solar Cell Integration

by

Tursunjan Yasin, Doctor of Philosophy

Utah State University, 2013

Major Professor: Dr. Reyhan Baktur
Department: Electrical and Computer Engineering

Transparent patch antennas are microstrip patch antennas that have a certain level of optical transparency. Highly transparent patch antennas are potentially suitable for integration with solar panels of small satellites, which are becoming increasingly important in space exploration. Traditional patch antennas employed on small satellites compete with solar cells for surface area. However, a transparent patch antenna can be placed directly on top of solar cells and resolve the issue of competing for limited surface real estate. For such an integration, a high optical transparency of the patch antenna is required from the solar cells' point of view. On the other hand, the antenna should possess at least acceptable radiation properties at the same time.

This dissertation focuses on some of the most important concerns from the perspective of small satellite applications. For example, an optimization method to simultaneously improve both optical transparency and radiation efficiency of the antenna is studied. Active integrated antenna design method is extended to meshed patch applications in an attempt to improve the overall power efficiency of the front end communication subsystem. As is well known, circular polarization is immune from Faraday rotation effect in the ionosphere and thus can avoid a 3-dB loss in geo-satellite communication. Therefore, this research also aims to present design methods for circularly polarized meshed patch antennas. Moreover, a

meshed patch antenna capable of supporting a high communication data rate is investigated. Lastly, other types of transparent patch antennas are also analyzed and compared to meshed patches. In summary, many properties of transparent patch antennas are examined in order to meet different design requirements.

(98 pages)

Public Abstract

Transparent Antennas for Solar Cell Integration

by

Tursunjan Yasin, Doctor of Philosophy

Utah State University, 2013

Major Professor: Dr. Reyhan Baktur
Department: Electrical and Computer Engineering

Transparent patch antennas have a certain level of optical transparency. Highly transparent patch antennas can be integrated with the solar panels of small satellites, which are becoming increasingly important in space exploration. Traditional patch antennas, which are not transparent, are employed on small satellites and compete with solar cells for surface area. But a transparent patch antenna can be placed directly on top of the solar cells and alleviate the issue of limited surface real estate. For such an integration, a high optical transparency of the patch antenna is required from the solar cells' point of view since the solar cells under the meshed patch need sufficient solar light to generate adequate electric power. On the other hand, the antenna should possess at least acceptable electrical properties at the same time so that it can radiate properly and efficiently.

This dissertation proposes different meshed patch antenna designs that meet some specific requirements. For example, an optimization method to improve both the optical transparency and radiation efficiency of the antenna is investigated. Similarly, this study also includes circular meshed patch antenna with harmonic suppression functionality, which can help improve the system's overall power efficiency such that the power generated by the solar cells would be efficiently utilized by the front end. Other studies are also reported

such as the meshed patch antenna with enhanced bandwidth and patch antennas made from transparent conductors, such as transparent conductive oxides films.

To my sweet daughter, Sabina ...

Acknowledgments

It would not be possible for me to finish my dissertation without the guidance of my committee members, help from my friends, and support from my family and wife.

In particular, I am profoundly indebted to my supervisor, Dr. Reyhan Baktur, who has been a steady influence throughout my Ph.D career. She has alwasys been patient and encouraging, especially in times of difficulties. Her expertise in her field and critical insights into new challenges have been one of the most important factors for me to make smooth progress in this research. And her impressive ability to balance research interests and personal pursuits has made me interested throughout.

I am grateful to the other members of my committee, Dr. Bela Fejer, Dr. Bedri Cetiner, Dr. Edmund Spencer, Dr. Jacob Gunther, and Dr. Doran Baker, for their insightful comments on my work. In addition, I would like to thank the ECE Department Head, Dr. Todd Moon, for being very supportive all the time.

I would also like to thank my colleagues in our research group, such as Tim Turpin, Mahmoud Nada, Ali Khoshniat, and Muhammad Rafiq, for their valuable discussions and efforts to make the dull office area a fun place to work.

I would like to express my deep appreciation to my parents, brother, and sister, who have been an important and indispensable source of spiritual support.

Finally, my special thanks go to my beloved wife, Gulistan, who has always been very understanding through the good times and bad. Without her persistent support, I would have never finished this dissertation.

Tursunjan Yasin

Contents

List of Tables

List of Figures

Acronyms

AIA	Active Integrated Antenna
AR	Axial Ratio
CP	Circular Polarization or Circularly Polarized
EMI	Electromagnetic Interference
HFSS	High Frequency Structure Simulator
ITO	Indium Tin Oxides
LHCP	Left-hand Circular Polarization or Left-hand Circularly Polarized
PA	Power Amplifier
PAE	Power Added Efficiency
PEC	Perfect Electric Conductor
RCS	Radar Cross Section
RHCP	Right-hand Circular Polarization or Right-hand Circularly Polarized
TCO	Transparent Conductive Oxides
TRL	Through-Reflect-Line
VNA	Vector Network Analyzer

Chapter 1

Introduction

Transparent patch antennas, as a special type of microstrip patch antennas have been studied for more than two decades. Their typical structure consists of a top-layer conductive patch, bottom-layer ground, and dielectric substrate in between. In this study, the top layer conductor and the dielectric substrate of the patch antenna are needed to be optically transparent. The conductor's transparency can be achieved by applying transparent conductive oxides (TCO) films, such as indium tin oxides (ITO), or by utilizing meshed sheets from regular conductors. For the see-through substrate, examples include regular glass, cover glass of solar panels, etc.

An important application of transparent patch antennas is their integration with the solar panels of small satellites, where limited surface area is an issue for mounting antennas, solar cells, and space instruments. This is of great significance for small satellites. Other possible applications include integration of antennas with window glass or car windshield.

This dissertation presents detailed studies on transparent patch antennas for small satellite applications. A simultaneous optimization method for both optical transparency and radiation efficiency of meshed patch antennas is proposed. Some practical antenna configurations are presented for specific application needs. In addition, feasibility study and analysis on transparent patch antennas made from ITO films are discussed as well.

1.1 Motivation

Small satellites (with a mass below 500 kg) have been identified as a major focus for future space exploration. They are cost-effective and can be launched to the orbit in a more economic way. Because of these advantages, which traditional satellites do not possess, they are widely employed in many space missions such as telecommunications, earth observations,

and a wide variety of scientific research. However, the size of a small satellite also limits the surface area for solar arrays and hence imposes constraints on the amount of available energy. As a result, design of the antenna system for small satellites, especially for cube satellites (CubeSats) or even smaller ones, remains one of the biggest challenges.

As part of the communication systems to handle command control, data download, and communications relay, antennas are very important components of satellites. Wire antennas such as crossed dipoles are the most popular antenna type in small satellite applications due to the ease of circular polarization (CP) configuration, wide range of operation frequency, and minimum occupation of surface area. But this type of antenna needs a complicated deployment mechanism, which may cause failure in communication and thus possible loss of the entire satellite. Another type of antennas frequently used on small satellites are conventional microstrip patch antennas. Despite their advantages of being low-profile, cost-friendly, and highly reliable, their application on small-sized satellites has been limited primarily because the use of patch antennas inevitably leads to reduction in solar array capacity of satellites.

As a solution to those challenges , highly transparent patch antennas backed with solid ground plane can be employed in small satellite applications. These antennas are electrically similar to conventional patch antennas and possess the same advantages. Furthermore, they provide high optical transparency, which is essential for the solar cells. Therefore, they can be placed directly on top of the solar panel without affecting the solar cells' functionality.

1.2 Literature Review

Lots of research efforts are made on antenna integration with solar cells in order to achieve both good antenna performance and maximized solar array capacity. It has been reported that a patch antenna can be placed under solar cells to obtain compatibility of antennas and solar cells [1]. However, this method involves a complicated multi-layered structure. Solar panel integrated slot antennas [2] seem to be a good solution to this issue. But the major drawback is that slot antennas have to be located in the gap between solar cells, significantly restricting design flexibility, especially for array configuration. However,

highly transparent patch antennas possess the potential to become the most promising antenna option for solar cell integration.

A method for fabricating transparent antennas is to create them from conductive mesh structure [3]. Some preliminary studies have addressed that meshed patch antennas mounted onto transparent substrates tend to have degraded properties, such as lower gain and higher backward radiation [4]. Clasen and Langley demonstrated another example, where meshed patch antennas were integrated into transparent substrates such as car windshield, and ended up with the similar conclusion [5]. Further studies suggested a complex trade-off between meshed patch antennas' properties: the bandwidth and cross-polarization level can be improved by sacrificing the gain [6] and a low radar cross section (RCS) can be achieved if the gain and bandwidth are compromised [7]. In a more detailed study on meshed patch antennas, Turpin proposed a guideline to optimize the design of meshed patch antennas [8], with which a meshed patch antenna of high transparency (93%) was realized and integrated on solar cells, and its radiation properties were comparable to those of solid patch antennas.

An alternative approach for constructing transparent antennas is to apply transparent conductive films, such as ITO films, onto see-through substrates. This method generally involves inconvenient special treatment during or after fabrication process. Additionally, conductive films of this type are usually lossy, especially if high transparency is required, due to its inherent material limitations [9, 10]. Although the hybrid ITO, multi-layered combination of copper and ITO, can improve the electrical properties, its transparency is compromised [11]. Another approach is to deposit highly conductive coating, usually not transparent, onto the most important area of the antenna where the highest current density occurs [12]. This, however, reduces the transmittance of the visible light as well.

However, these background works only provide the initial feasibility study on transparent patch antennas, although their applications may be very promising owing to the multi-functionality of being effective radiators with high optical transparency. For meshed patch antennas, most studies have only focused on rectangular patches in spite of the di-

versity of patch geometries. In fact, of the same importance are circular patches, on which Clasen and Langley proposed some important guidelines for designing mesh patterns [13]. According to her work, the mesh geometry of circular patch antennas should support the current paths of a certain radiation mode such that the other modes can be suppressed to some extent. But study on the relationship of transparency and radiation properties is still insufficient. In addition, the current literature is lack of some crucial aspects of the study on meshed patch antennas. For example, integration with other electronics such as power amplifiers, realization of CP with simple antenna structures, bandwidth improvement for high data rate, and array configurations are all needed in practical applications. On the other hand, a more systematic and comprehensive understanding of transparent patch antennas made from conductive films is also needed in order to apply such antennas in application where their advantages can be fully utilized.

1.3 Dissertation Overview

This dissertation is focused on transparent patch antenna design for integration with solar panels of small satellites and organized in the paper format. It consists of six individual papers, each as an independent chapter, from Chapter 2 to Chapter 7.

In the first paper, an optimization design guideline for meshed patch antennas is given. Effects of different parameters of the mesh geometry on the antenna performance is discussed. Based on this, a method to simultaneously improve both the optical transparency and the radiation efficiency is obtained.

The second paper presents a design method for circular meshed patch antennas with harmonic suppression capability, which can be integrated with power amplifiers in a compact manner. The antennas' input impedance is of interest since it is a sufficient measure to verify whether the design is successful.

Two different designs to realize CP for meshed patch antennas are reported in the third and fourth papers. The straight microstrip proximity feed line used in the third paper requires two square meshed patches to yield CP. In the fourth paper, a single meshed patch antenna (nearly square) is excited with a Y-shaped coupling feed, which has a much simpler

feeding mechanism but would cast a small amount of shadow onto solar cells in practical applications.

The fifth paper is about bandwidth enhancement for meshed patch antennas, where three square meshed patches of slightly different sizes are utilized to generate an improved bandwidth. The radiation pattern is compromised moderately due to the coupling effect of the closely spaced meshed patch elements.

In the last paper, transparent patch antennas made from TCO films are examined and compared to meshed patch antennas. TCO materials, although expensive, have a promising potential for transparent antenna applications at high frequencies (e.g. K- or Ku-band).

References

[1] S. Vaccaro, C. Pereira, J. Mosig, and P. de Maagt, "In-flight experiment for combined planar antennas and solar cells (solant)," *IET Microwaves, Antennas & Propagation*, vol. 3, no. 8, pp. 1279–1287, 2009.

[2] M. N. Mahmoud, "Integrated solar panel antennas for cube satellites," Master's thesis, Utah State University, Logan, UT, 2010.

[3] R. N. Simons and R. Q. Lee, "Feasibility study of optically transparent microstrip patch antenna," *IEEE Antennas and Propagation Society International Symposium*, vol. 4, pp. 2100–2103, 1997.

[4] K. Ito and M. Wu, "See-through microstrip antennas constructed on a transparent substrate," *7th IET International Conference on Antennas and Propagation*, pp. 133–136, 1991.

[5] G. Clasen and R. Langley, "Meshed patch antenna integrated into car windscreen," *Electronics Letters*, vol. 36, no. 9, pp. 781–782, 2000.

[6] ——, "Meshed patch antennas," *IEEE Transactions on Antennas and Propagation*, vol. 52, no. 6, pp. 1412–1416, 2004.

[7] X. He, S. Gong, Y. Ji, and Q. Liu, "Meshed microstrip patch antennas with low RCS," *Microwave and Optical Technology Letters*, vol. 46, no. 2, pp. 117–120, 2005.

[8] T. W. Turpin, "Meshed patch antennas integrated on solar cell - a feasibility study and optimization," Master's thesis, Utah State University, Logan, UT, 2009.

[9] N. Outaleb, J. Pinel, M. Drissi, and O. Bonnaud, "Microwave planar antenna with RF-sputtered indium tin oxide films," *Microwave and Optical Technology Letters*, vol. 24, no. 1, pp. 3–7, 2000.

[10] P. Prajuabwan, S. Porntheeraphat, A. Klamchuen, and J. Nukeaw, "ITO thin films prepared by gas-timing RF magnetron sputtering for transparent flexible antenna," *2nd IEEE International Conference on Nano/Micro Engineered and Molecular Systems*, pp. 647–650, 2007.

[11] F. Colombel, X. Castel, M. Himdi, G. Legeay, S. Vigneron, and E. M. Cruz, "Ultrathin metal layer, ITO film and ITO/Cu/ITO multilayer towards transparent antenna," *IET Science, Measurement & Technology*, vol. 3, no. 3, pp. 229–234, 2009.

[12] H. J. Song, T. Y. Hsu, D. F. Sievenpiper, H. P. Hsu, J. Schaffner, and E. Yasan, "A method for improving the efficiency of transparent film antennas," *IEEE Antennas and Wireless Propagation Letters*, vol. 7, pp. 753–756, 2008.

[13] G. Clasen and R. Langley, "Gridded circular patch antennas," *Microwave and Optical Technology Letters*, vol. 21, no. 5, pp. 311–313, 1999.

Chapter 2

Optimized Design Method for Highly Transparent Meshed Patch Antennas Backed by Solid Ground Plane

Abstract

Rectangular and circular patch antennas fabricated from meshed conductors and backed with solid ground planes are analyzed in this paper. Because of the meshing, the antennas are optically transparent, where the transparency is determined by the mesh geometry. It is found that although there is a compromise between the antennas efficiency and the optical transparency of the meshed patch, it is possible to optimize the antenna with both radiation properties and the optical transparency by carefully designing the mesh geometry. A refined mesh with thin linewidth increases both antenna performance and transparency. Additionally, it is found that the reduction of certain mesh lines increases the optical transparency with minimal hindrance to the antennas efficiency, leading to further enhancement to the see-through percentage. Although it is possible to refine mesh lines to improve antennas efficiency or gain, it is seen that there is a limit for such an optimization method. The limit is closer to the efficiency of a solid patch for a lower transparency, whereas being lower for increased transparency. Cross polarization level was also examined and there was no significant effect on such parameter due to meshing.

2.1 Introduction

Meshed patch antennas have similar properties to normal microstrip patch antennas [1] while using less metal [2, 3] and being optically transparent [4–6]. Because of having less metal hence less heat dissipation and being optically transparent, they find applications in integration with window glass [2] and solar cells [4]. Other methods to design planar transparent antennas, such as using silver coated polyester (AgHT) [7] and indium tin oxides

(ITO) films [8–10], were reported. But the optical transparency of those antennas is not high enough for applications such as solar cell integration, especially at lower GHz frequencies. Alough Clasen et al. presented a comprehensive study on meshed patch antennas with solid and meshed ground plane, it only considered mesh lines with fixed linewidth [1]. Other studies on meshed antennas did not capture the effect of linewidth on the antenna functionalities [2, 11]. As will be shown in this paper, the width of the mesh lines is an important design parameter, and it is practical to easily create different mesh geometries using conductive ink. This paper aims to present a design guideline of highly transparent meshed antennas that can be potentially integrated on top of solar cells. Majority of this study is through experiments and the operational frequencies are around 2.2 GHz for rectangular meshed antennas and 2.5 GHz for circular meshed antennas. But the design principle is also valid for higher frequencies.

2.2 Meshed Patch Antenna Topology

The mechanism of a transparent meshed patch antenna is straightforward, where the optical signals can transmit through the openings of the mesh and the conductor still acts as a valid radiator at microwave frequencies. This, of course, requires that there are enough mesh lines to prevent significant leakage of microwave signals.

Although meshed patch antennas find applications in many areas [2, 11], the main interest of this study is to provide a transparent antenna design to be integrated with the solar panels of Cube Satellites (CubeSats) to save very limited surface real estate. Typically, the solar panel of a CubeSat has a solid metal backing (i.e. metallic shielding of the satellite), as illustrated in Fig. 2.1, and this metal plane can serve as the ground plane for the antenna whereas the photovoltaic layers and solar cell cover glass can serve as the substrate for the antenna. Therefore, this paper only studies the meshed antenna backed by a solid ground plane.

The mesh patterns can be designed following the guidelines presented in [3], where the mesh geometry of the antenna should follow the current paths of a certain radiation mode. This assures not only predictable antenna properties but also suppression of undesired

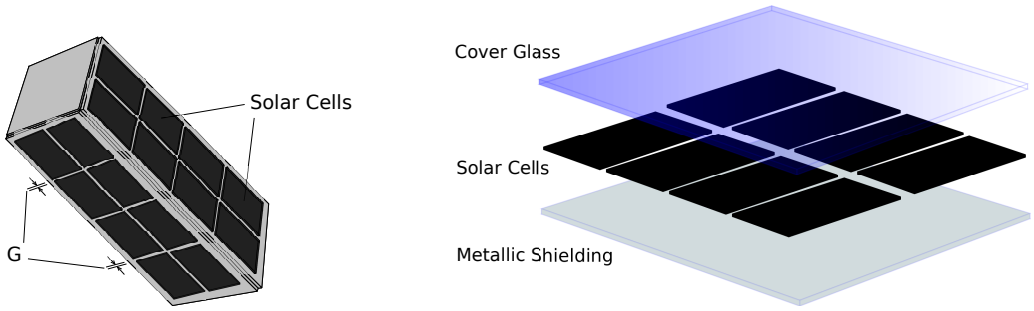

(a) (b)

Fig. 2.1: Solar panel of a CubeSat: a) isometric view of a CubeSat; b) solar panel structure.

radiation modes. This paper focuses on rectangular and circular meshed patches that primarily radiate the fundamental mode, as depicted in Fig. 2.2, due to their relatively simple mesh patterns. It can be seen that a meshed patch antenna consists of two sets of mesh lines. The first set of lines are responsible for carrying the desired currents whereas the second set are orthogonal to the current path lines to form a patch.

The optical transparency of such meshed patches is defined as the percentage of the see-through area of the patch. For example, the formula to calculate the transparency (T_{rect}) of a rectangular meshed patch which has dimensions of W (width) by L (length) is as follows:

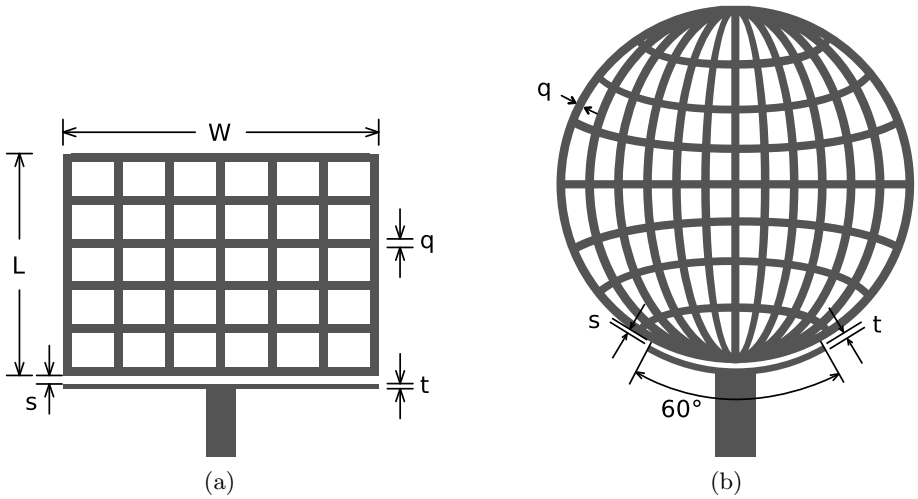

(a) (b)

Fig. 2.2: T-coupled meshed patch antennas: a) rectangular; b) circular.

$$T_{rect} = (1 - \frac{A_{conductor}}{A_{patch}}) = [\frac{L \cdot W - q(M \cdot L + N \cdot W) + q^2 \cdot M \cdot N}{L \cdot W}] \cdot 100\%, \tag{2.1}$$

where M is the number of lines parallel to the length of the patch, N is the number of lines orthogonal to the length of the patch, and the uniform mesh line thickness is q (Fig. 2.2a). The calculation of a circular meshed patch (Fig. 2.2b) cannot be achieved directly using a simple mathematical equation due to irregular curves involved in the mesh geometry. However, this challenge can be overcome by utilizing basic image processing functions in Matlab. The digital image of a circular meshed patch can be analyzed to calculate the transparency (T_{circ}) with the following equation:

$$T_{circ} = (1 - \frac{N_{pixel}^{cond}}{N_{pixel}^{patch}}) \cdot 100\%, \tag{2.2}$$

where N_{pixel}^{cond} and N_{pixel}^{patch} are, respectively, the numbers of pixels in the conductor area and in the entire circular patch area.

As the targeted potential application of the meshed antennas in this study is solar cell integration, it is important to choose a practical feeding method. Most common feed designs [12] require either drilling holes through solar cells or altering the antenna geometry. Therefore, we chose to apply a proximity coupling method [13–15], as illustrated in Fig. 2.2, where a T-shaped coupling line parallel to the periphery of the mesh is employed to excite the antenna. This feeding method potentially provides two degrees of freedom for tuning: the branch thickness t and the spacing s as marked for both rectangular and circular meshed patches in Fig. 2.2. Although the angle of the arch that is formed by the two branches can be the third parameter for impedance matching in the case of circular meshed patches, it was found that the optimal coupling performance can be achieved when it is 60^{o} [13]. Other benefits of this feeding technique include low insertion loss in dual port application [15] and improved gain and bandwidth [16]. It is true that such a feed line may decrease the overall transparency of the antenna. But the thick microstrip line can be placed on top of the

cover glass above one of the gaps (G in Fig. 2.1a) between solar cells, leaving the thinner branches of the T-shaped line to be the only decreasing factor on the transparency. This way, such a decrease is manageable and can be overcome by improving the transparency of the meshed patch.

2.3 Rectangular Meshed Patch Antennas

It has been reported that the resonant frequency, gain, and efficiency of a meshed patch antenna decrease when transparency of the antenna is increased [2, 3]. This means one has to compromise the optical transparency and the efficiency of a meshed patch antenna. Clasen also pointed out that the input impedance of a meshed patch antenna becomes higher as its transparency increases, making it more challenging for impedance matching. These previously published studies, however, did not consider the effect of the linewidth on the antenna performance. All those studies have varied the transparency by changing the number of lines while keeping the linewidth as a constant value. It is clear from (2.1) that one may achieve a more transparent antenna with very thin mesh lines, and therefore it is important to understand how the linewidth (q) affects the radiation properties of a meshed antenna.

A typical method to perform a parametric study on an antenna is through simulation followed by an experimental verification. This process has its advantage of reducing unnecessary time and effort in testing an ineffective prototype. Our approach, however, is through experiments for two reasons: 1) we have developed a fast and low-cost antenna prototyping method through printing with conductive ink [17]; 2) the parameters to be studied are limited and relatively simple, and therefore one may skip the step of simulation. The experimental studies were set up to examine how the linewidth of the meshes affects the antenna's performance. Two types of printing methods were used. The first type is screen printing with conductive ink, where the antennas were printed directly on a plexiglass substrate. The second type is inkjet printing, where the conductive ink was printed on thin transparencies and the transparencies were assembled on the plexiglass.

2.3.1 Experiments with Screen Printed Probe Fed Meshed Patch Antennas

A set of four rectangular meshed patch antennas with the same optical transparency of 70% but different linewidth were screen printed onto plexiglass ($\epsilon_r = 2.6$, $tan\delta = 0.0057$, $h = 2.032$ mm) using a silver based conductive ink (124-46 by Creative Materials). The substrate (approximately 130 mm by 150 mm) was backed with copper tape to act as the ground plane of the antenna. The antennas have identical dimensions of 45 mm by 37 mm and were excited with a coaxial probe. The linewidth q was varied from 0.3 mm to 1.5 mm. It should be noted that the number of lines (M and N) were also adjusted in order to maintain a constant optical transparency.

The measured results are presented in Fig. 2.3, 2.4 and 2.5, where it is evident that the antenna radiation properties are improved with the reduced linewidth. It is seen from Fig. 2.3 that for a given transparency, the resonant frequency of a meshed patch approaches that of the solid patch of the same size as one refines the linewidth. Table 2.1 presents the inset distance of the probe of the antenna, and it shows that the input impedance of a meshed patch antenna becomes lower and approaches that of the solid patch of the same size as the mesh lines become thinner. The abnormality of the first data point from $q =$ 0.3 mm is most likely due to the loss rising from the inaccurate manufacturing process of screen printing. The printing technique pursued in those tests was not precise, and it was challenging to maintain smooth printed lines, especially when the lines were very thin. It is well known that non-smooth conductive lines are very lossy due to diffraction. Therefore, the loss factor due to non-smooth lines might have offset the improvement in the efficiency by refining lines.

Table 2.1: Feed point insert distance v.s. linewidth of rectangular meshed patches (45 mm by 37 mm).

Antenna	q (mm)	M	N	d (mm)
A	0.3	24	20	7.1
B	0.5	14	12	6.3
C	1.0	7	6	8.2
D	1.5	5	4	11.0

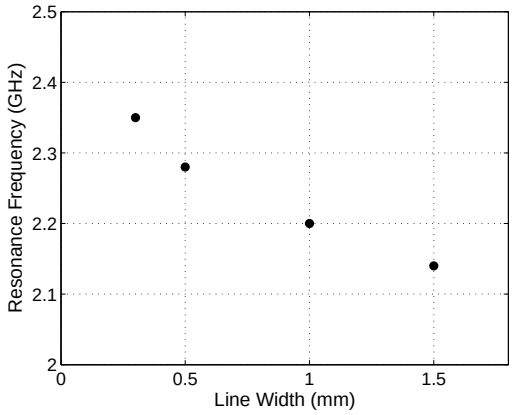

Fig. 2.3: Effect of linewidth on resonant frequency of rectangular meshed patch (T_{rect} = 70%).

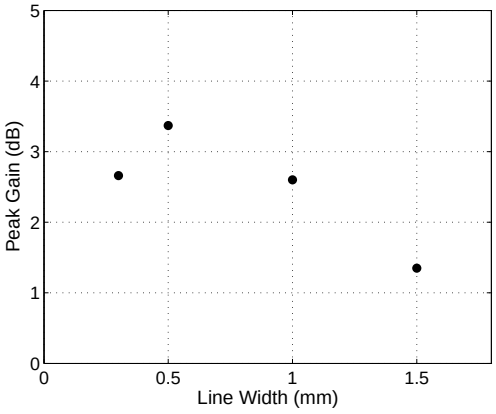

Fig. 2.4: Effect of linewidth on peak gain of rectangular meshed patch (T_{rect} = 70%).

2.3.2 Experiments with Inkjet Printed Proximity Fed Meshed Patch Antennas

For a solid patch antenna, the current distribution of the fundamental mode is from one radiating edge to the other with higher density at the two non-radiating edges than in the center of the patch [1]. For a meshed patch antenna, the currents were distributed over the mesh lines that are parallel to the non-radiating edges of the patch [1]. We call these lines current path lines, and the number of these lines is M in Equation (2.1). It can be predicted that the more current path lines in a meshed patch, a better radiation property of the antenna can be achieved as such a mesh has closer resemblance to a solid patch in terms of current distribution.

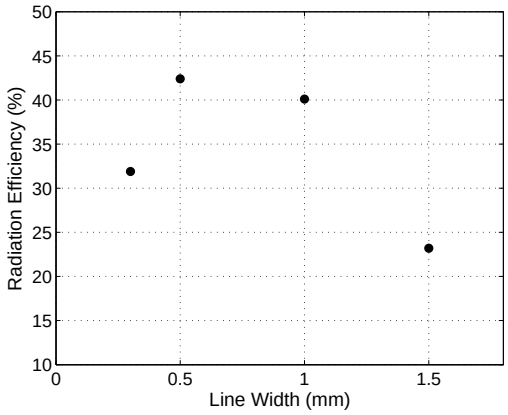

Fig. 2.5: Effect of linewidth on radiation efficiency of rectangular meshed patch (T_{rect} = 70%).

A straightforward method to achieve more current patch lines without sacrificing optical transparency is to refine mesh lines. In order to verify the prediction of more refined current path lines yielding a more effective antenna, and to overcome a precision in prototyping, four meshed patch antennas were prototyped using inkjet printing method that yields much smoother lines. Four rectangular meshed patches (45.6 mm by 38.6 mm) with a fixed number (N) of lines orthogonal to the current path lines were inkjet printed using the nanosilver aqueous dispersive conductive ink (Metalon JS-B25P by Novacentrix) on a thin polyethylene terephthalate (PET) film. The meshes were then assembled onto the same plexiglass substrate as in 2.3.1. The number of the current path lines and the linewidth were varied to maintain the transparency in the vicinity of 70% . The linewidth of the current patch lines and the orthogonal ones are remained the same. The details of these antennas' geometries are given in Table 2.2. The antennas were excited using the proximity T-coupling line (Fig. 2.2a), where the length of the T-coupling line is the same as the width of the antenna. The two parameters t and s were chosen to be 1 mm and 0.6 mm to achieve a good impedance matching.

The measurements of resonance frequency, gain and radiation efficiency are plotted in Fig. 2.6, 2.7 and 2.8. It can be observed that, for a given transparency, all those parameters can be improved by refining the mesh lines. Thinner mesh lines give rise to more current

Table 2.2: Geometry of inkjet printed rectangular meshed patch antennas (45.6 mm by 38.6 mm).

Antenna	q (mm)	M	N	T_{rect} (%)
A	0.4	18	9	76
B	0.5	14	9	74
C	0.6	12	9	72
D	0.7	10	9	71

path lines and hence more effective antenna. In fact, it is seen that the transparency of the patch with the thinner lines are higher than those with thicker lines. This further confirms the conclusion that it is possible to obtain an effective antenna with higher transparency by refining its mesh lines.

2.3.3 Effect of Orthogonal Lines

The discussion and results in 2.3.2 show that a meshed antenna with more current path lines yields a higher efficiency. Previous research has also suggested the similar claim that the current path lines are more important than the horizontal lines [6]. This suggests that reducing the number of orthogonal lines may not affect antenna properties and that one can achieve extra optical transparency by eliminating some lines.

A simulation study using Ansys's High Frequency Structure Simulator (HFSS) was performed to verify the effect of the horizontal lines. The meshed antenna under study has

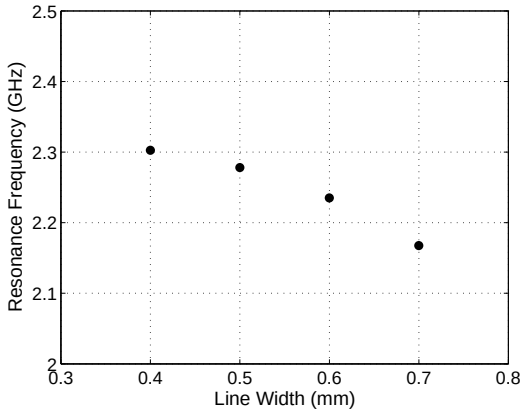

Fig. 2.6: Effect of current path lines on resonant frequency of rectangular meshed patch ($T_{rect} \approx 70\%$).

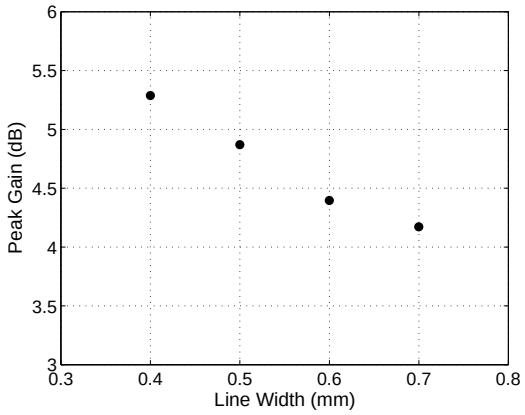

Fig. 2.7: Effect of current path lines on peak gain of rectangular meshed patch ($T_{rect} \approx 70\%$).

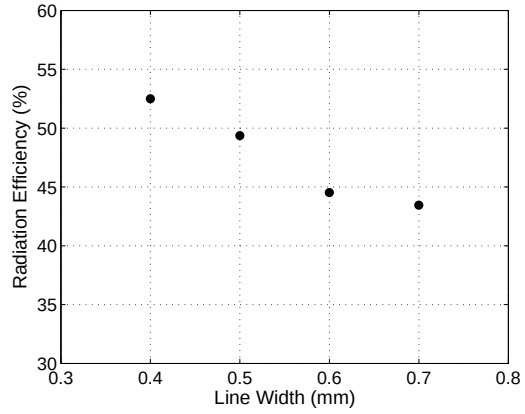

Fig. 2.8: Effect of current path lines on radiation efficiency of rectangular meshed patch ($T_{rect} \approx 70\%$).

a fixed width and length of 45 mm and 37 mm, and the substrate is the same Plexiglas material as in the previous two studies. The mesh geometry consists of 25 current path lines, and the number of orthogonal lines was varied from 20 to 6 while the linewidth was fixed as 0.3 mm; consequently, the optical transparency is ranged from 70% to 79%. The efficiency of these antennas is listed in Table 2.3. It is observed that reducing the horizontal lines to a certain degree does not affect the antenna's performance significantly. On the contrary, Table 2.3 suggests reducing horizontal lines yields slightly increased antenna efficiency. This can be explained through checking the resonant frequency (F_r in Table 2.3). It is seen F_r is lower for meshed patches with more horizontal lines. This is because when there are

more horizontal lines, there are more possible current paths by meandering through vertical and horizontal lines. These meander paths are longer than vertical lines and therefore give rise to lower resonant frequencies. At the same time, longer lines mean higher resistance, and therefore lower efficiency. This study suggests another method to optimize a meshed antenna's optical transparency without sacrificing its efficiency.

We have also noticed that keeping horizontal lines to minimum instead of fully eliminating them as in some studies [1] helps to maintain good antenna pattern and efficiency. In the case of this particular study in Table 2.3, the antenna's properties start to be unstable after reducing horizontal lines to less than 6.

2.3.4 Effect of Meshing

The experiments in 2.3.1 and 2.3.2 showed that the gain and efficiency of a meshed patch antenna can be improved by refining the linewidth for a given transparency. It may give one an impression that it is possible to achieve a meshed antenna as effective as the solid patch without meshing as long as one keeps the linewidh very thin. This could have been true if the mesh material is a perfect electric conductor. For a normal conductor such as copper, there is a gain loss due to meshing. In addition, when the mesh lines are as thin as to be comparable with the microwave skin depth, the lines will exhibit high loss that will further reduce the antenna's gain.

Using the optimization method discussed earlier, four meshed copper antennas with the same patch size but different transparencies were designed on the substrate ($\epsilon_r = 2.6$,

Table 2.3: Effect of orthogonal lines on antenna properties of rectangular meshed patches (45 mm × 37 mm).

Mesh Geometry	q (mm)	T_{rect} (%)	F_r (GHz)	$Eff.$ (%)
25 by 20	0.3	69.8	2.32	72.2
25 by 16	0.3	72.5	2.33	72.9
25 by 12	0.3	75.2	2.36	73.1
25 by 8	0.3	78	2.4	73.6
25 by 6	0.3	79.3	2.38	73.7

$tan\delta = 0.002$, $h = 2.032$ mm) backed with solid copper plane to act as the ground, and they were simulated and compared against their solid counterpart using HFSS. The purpose of this study was to examine the meshing effect on the gain of copper patch antennas. The simulation results are listed in Table 2.4, where it can be seen that the gain loss of the antenna due to meshing is close to 2.5 dB for the 95% transparent meshed patch and that such loss decreases with a reduced transparency. Therefore, it can be concluded that meshing itself in practical design of meshed patch antennas results in an inevitable loss that depends on the patch transparency and becomes more obvious when the transparency is higher.

2.4 Inkjet Printed Circular Meshed Patches

Circular meshed patch antennas are of the same importance as the rectangular ones. When designing circular meshed patches, the mesh geometry needs to be such that they support the current patterns of the desired resonant mode [3]. Consequently a circular meshed antenna that supports the fundamental mode has a mesh pattern as shown in Fig. 2.2b. It is found that simulating a circular meshed antenna with refined linewidth takes a substantial amount of time and memory of a moderate personal computer, whereas direct prototyping using inkjet printing is much faster, cheaper, and easier. Therefore, the following studies on the circular meshed antennas were through experiments.

2.4.1 Tradeoff between the Optical Transparency and Radiation Properties of a Circular Meshed Patch Antenna with Fixed Linewidh

Six circular meshed patches of the same linewidth but different line numbers were inkjet

Table 2.4: Effect of meshing on the gain of rectangular meshed copper patch (45 mm by 37 mm).

$G_{0,solid}$ (dB)	7.32			
T_{rect} (%)	70	80	90	95
Linewidth q (mm)	0.133	0.136	0.100	0.100
$G_{0,meshed}$ (dB)	6.52	6.08	5.25	4.90
$G_{0,meshed}$ - $G_{0,solid}$ (dB)	-0.80	-1.24	-2.07	-2.42

printed on the PET films and then assembled onto the plexiglass substrate that were the same as in Section 2.3.1. The conductive ink was Metalon JS-B25P by Novacentrix. The transparency of these antennas was varied from 39.2% to 75.6% by changing the number of lines. All these antennas were fed using the T-coupling line (Fig. 2.2b), where the two parameters t and s were chosen to be 0.5 mm and 0.3 mm for a good impedance matching. The measurement results led to the same conclusion as in [2], where the tradeoff between the optical transparency and the radiation properties is that one has a less effective antenna for an increased transparency.

2.4.2 Effect of the Linewidth on Antenna Efficiency

In this study, a set of eight circular meshed patches of the same transparency (60%) but different linewidths were fabricated using the inkjet printing method. The conductive ink was Metalon JS-B25P by Novacentrix. The linewidth of these antennas were varied from 0.46 mm to 0.89 mm. Their measured parameters were compared, and the results are plotted in Fig. 2.9, 2.10 and 2.11. It is seen that, although there is some slight fluctuation in the data, the general trend of numbers suggests the same conclusion as those for the rectangular meshed antennas. That is, by refining mesh lines, one can achieve a more effective transparent antenna that has its properties closer to the non-meshed solid patch.

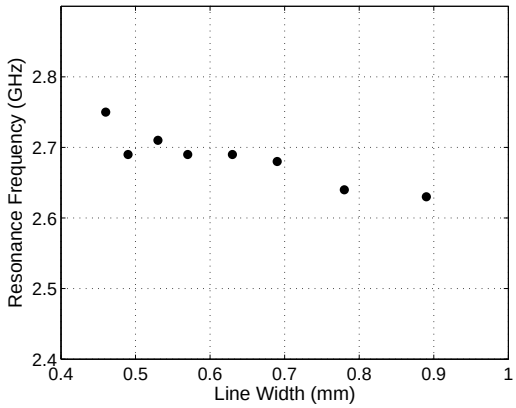

Fig. 2.9: Effect of linewidth on resonant frequency of circular meshed patch ($T_{circ} = 60\%$).

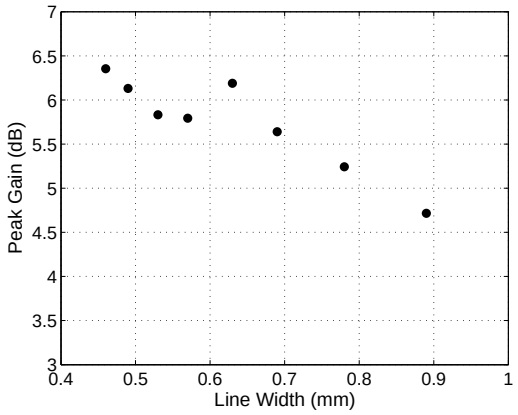

Fig. 2.10: Effect of linewidth on peak gain of circular meshed patch ($T_{circ} = 60\%$).

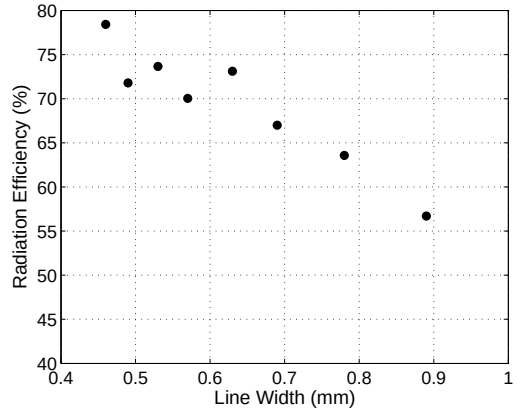

Fig. 2.11: Effect of linewidth on radiation efficiency of circular meshed patch ($T_{circ} = 60\%$).

2.4.3 Cross Polarization Level

We have examined the cross polarization level for both rectangular and circular meshed patch antennas through simulation study. It is seen that for a fixed transparency, refining the mesh lines does not reduce the cross polarization level. Reduction of horizontal lines also does not seem to significantly affect the cross polarization. Overall, the cross polarization level for meshed patch antennas is not significantly worse than a solid patch antenna. Therefore, one does not need to concern the trade-off between the transparency and cross polarization level.

2.5 Discussions and Conclusion

Experiments performed on both rectangular and circular meshed patch antennas yield the consistent conclusion that one can optimize both transparency and efficiency of a meshed antenna by refining the linewidth. It is noted that the efficiency of the conductive ink printed antennas were low. The reasons for this are slightly different for the two types of printing. For the screen printed antennas, the low efficiency is due to the quality of the ink, thickness of the ink layer, and the smoothness of the printed lines. The conductive ink is not as conductive as a normal conductor such as copper, even after being cured. In most printing methods, the thickness of the ink layer is comparable to the skin depth , and therefore high loss is exhibited. As discussed in Section 2.3.1, it is challenging to achieve sufficiently smooth lines using screen printing, and consequently the loss due to the edge diffraction is unavoidable. For the inkjet printed meshes, the first two reasons of lower efficiency are the same as in the screen printing, whereas the third one is due to the antenna assembly. Inkjet printing yields smooth lines, but using a normal commercial inkjet printer (e.g. Epson C88), one has to print the structure on a transparency and then assemble the transparency onto the antenna substrate. In doing so, an extra layer of substrate is introduced as well as some air in between transparency and the plexiglass substrate. It should be also noted that, in both types of prototyping, we used copper tape as the ground plane, and this may introduce extra loss. Finally, the plexiglass has a higher loss tangent and it further contributes to low efficiency.

When refining the linewidth to improve a meshed patch antenna's efficiency, there is an upper bound of efficiency for each transparency. There is a loss due to meshing a non-perfect conductor. Such a loss is higher for a meshed antenna with higher transparency. While such loss is less than 1 dB for a 70% transparent rectangular meshed patch antenna, it is about 2.5 dB for a 95% transparent rectangular antenna. It is also observed through simulation study that meshing a patch antenna does not reduce the cross polarization level. The cross polarization level is also not affected significantly by refining the mesh or reducing the horizontal lines.

Although the experimental studies in this paper were for antennas with lower transparencies, the results drawn from the measurements can be applied to achieve a highly transparent antenna with optimized gain. A transparency higher than 90% (in particular, as high as 95%) has a great future application in CubeSat technology, where one may integrate such an antenna directly on top of the solar cells. Printing a 0.1 mm line using either an inkjet printer, or other methods, is highly feasible. One may also repeatedly print several times on the same line trace to increase the ink layer to overcome the loss associated with skin depth. When the quality of the ink and printing are not loss factors, our prediction is that one can realistically print an S-band (this band is of interest because it enables a CubeSat to use cell phone technology in its radio) 95% transparent antenna with 0.1 mm mesh lines on a low loss substrate with a reasonable thickness and achieve a gain close to 5.0 dB or an efficiency close to 60%. A transparency of 95% is a highly applicable number for solar cell integration. With such a transparency, a typical S-band antenna only casts less than 3% shadow on a 10 cm by 10 cm panel, and such a shadow is comparable to the one cast by the traditional wire antennas after being deployed. Most solar cells for space applications have a thin cover glass and can serve as the substrate for the antenna, although such glass is often too thin to produce an efficient S-band antenna. However, a new type of silicone cover glass has been developed and is gaining popularity (www.vst-inc.com). Besides optical and mechanical advantages, those silicone cover material is thicker and may be a good choice to facilitate antenna integration.

It is known that the active junctions of solar cells will affect the antenna's performance. Though not the scope of this paper, our initial tests yield yet non-conclusive but at least 2 dB gain loss of the antenna due to the solar cells beneath it [17]. Besides possible solar cell integration, the optimized design method for meshed antennas presented in this paper helps yield the most effective windshield antenna with least metal weight for vehicular communication [2].

References

[1] G. Clasen and R. Langley, "Meshed patch antennas," *IEEE Transactions on Antennas and Propagation*, vol. 52, no. 6, pp. 1412–1416, 2004.

[2] ——, "Meshed patch antenna integrated into car windscreen," *Electronics Letters*, vol. 36, no. 9, pp. 781–782, 2000.

[3] ——, "Gridded circular patch antennas," *Microwave and Optical Technology Letters*, vol. 21, no. 5, pp. 311–313, 1999.

[4] T. W. Turpin and R. Baktur, "Meshed patch antennas integrated on solar cells," *IEEE Antennas and Wireless Propagation Letters*, vol. 8, pp. 693–696, 2009.

[5] K. Ito and M. Wu, "See-through microstrip antennas constructed on a transparent substrate," in *Seventh International Conference on Antennas and Propagation.* IET, 1991, pp. 133–136.

[6] M.-S. Wu and K. Ito, "Basic study on see-through microstrip antennas constructed on a window glass," in *IEEE Antennas and Propagation Society International Symposium.* IEEE, 1992, pp. 499–502.

[7] H. J. Song, T. Y. Hsu, D. F. Sievenpiper, H. P. Hsu, J. Schaffner, and E. Yasan, "A method for improving the efficiency of transparent film antennas," *IEEE Antennas and Wireless Propagation Letters*, vol. 7, pp. 753–756, 2008.

[8] C.-T. Lee, C.-M. Lee, and C.-H. Luo, "The transparent monopole antenna for wcdma and wlan," in *IEEE Annual Wireless and Microwave Technology Conference*, 2006, pp. 1–3.

[9] F. Colombel, X. Castel, M. Himdi, G. Legeay, S. Vigneron, and E. M. Cruz, "Ultra-thin metal layer, ito film and ito/cu/ito multilayer towards transparent antenna," *IET Science, Measurement & Technology*, vol. 3, no. 3, pp. 229–234, 2009.

[10] N. Guan, H. Furuya, K. Himeno, K. Goto, and K. Ito, "A monopole antenna made of a transparent conductive film," in *IWAT '07 International Workshop on Antenna Technology: Small and Smart Antennas Metamaterials and Applications*, 2007, pp. 263–266.

[11] X. He, S. Gong, Y. Ji, and Q. Liu, "Meshed microstrip patch antennas with low rcs," *Microwave and Optical Technology Letters*, vol. 46, no. 2, pp. 117–120, 2005.

[12] R. N. Simons and R. Q. Lee, "Feasibility study of optically transparent microstrip patch antenna," in *IEEE Antennas and Propagation Society International Symposium*, vol. 4. IEEE, 1997, pp. 2100–2103.

[13] L. Zhu and K. Wu, "Line-to-ring coupling circuit model and its parametric effects for optimized design of microstrip ring circuits and antennas," in *IEEE MTT-S International Microwave Symposium Digest*, vol. 1. IEEE, 1997, pp. 289–292.

[14] ——, "A joint field/circuit model of line-to-ring coupling structures and its application to the design of microstrip dual-mode filters and ring resonator circuits," *IEEE Transactions on Microwave Theory and Techniques*, vol. 47, no. 10, pp. 1938–1948, 1999.

[15] D. G. Kurup and A. Rydberg, "Amplifying active reflect-antenna using a microstrip-t coupled patch - design and measurement," *IEEE Transactions on Microwave Theory and Techniques*, vol. 51, no. 8, pp. 1960–1965, 2003.

[16] J.-C. Liu, H. C. Wu, M. S. Chiang, and H.-Y. Tsou, "T-coupled circular microstrip antenna with h-shaped aperture for bandwidth and radiation-gain improvements," *Microwave and Optical Technology Letters*, vol. 37, no. 6, pp. 414–417, 2003.

[17] J. A. Arellano, "Inkjet-printed highly transparent solar cell antennas," M.S. thesis, Dept. ECE, Utah State University, Logan, UT, 2011.

Chapter 3

Circular Meshed Patch Antenna with Harmonic Suppression Functionality for Integration with Power Amplifiers

Abstract

A circular meshed patch antenna that is capable of effectively suppressing the 2nd and 3rd harmonics is presented. The design is simple and can be conveniently integrated with a power amplifier for reduced circuit size and increased power added efficiency of the amplifier. The harmonics suppressing capability of the antenna design is not sensitive to substrates and thus can facilitate the application of such an antenna on a wide range of materials such as car windshield and solar cells.

3.1 Introduction

Meshed patch antennas have similar properties as normal microstrip patch antennas [1] while using less metal [2] and being optically transparent [3, 4]. Because of having less metal, hence less heat dissipation and being optically transparent, they find applications in integration with window glass [2] and solar cells [3]. On the other hand, researchers have shown the concepts of an active integrated antenna (AIA), where the antenna is directly integrated with a power amplifier (PA) to reduce the size of the circuitry and to improve the power added efficiency (PAE) [5–15]. In order to achieve an effective active integration, it has been shown that the antenna geometry or its ground plane have to be modified to attain harmonic suppression [13,15]. This paper shows that the mesh geometry of a circular meshed patch antenna can also control the harmonic suppression and is more effective than the reported circular sector antenna [7, 10], which is so far one of the best antenna topologies in AIA design. In addition, the proposed meshed antenna can also be

designed on transparent substrates such as the cover glass of solar cells for cube satellite applications [3].

3.2 AIA Design for Circular Meshed Patch

3.2.1 Bases of Harmonic Suppression

The principles of AIA design and the need for the antenna's harmonics suppressing capability have been explained in a rich range of literature [8, 10, 11]. It has been shown that the higher harmonics of a patch antenna can be suppressed by destroying the radiation modes around the harmonics of the amplifier [10] or shifting the radiation modes away from higher harmonics, which can be achieved by significantly altering the current paths of resonant modes close to those harmonics [7]. The second approach results in almost purely reactive terminations of the modified antenna at its higher harmonics, which is desirable in the amplifier end.

The requirements for the meshed antenna design are as follows. The antenna needs to behave like its solid counterpart for the fundamental radiation mode, i.e. an effective radiator. At the same time, the mesh geometry is such that it allows the antenna to effectively suppress the higher harmonics of the PA. A typical meshed circular patch antenna is shown in Fig. 3.1(a), where the set of mesh lines from the back end (E1) to the front end (E2) correspond to the current paths of the fundamental mode. The other set of lines, which are orthogonal to the current path lines connect these current path lines to form a patch. Such a meshed patch antenna primarily promotes the fundamental mode [1]. However, the higher modes that coincide in the vicinity of higher harmonics can still be excited since the corresponding current paths, although slightly distorted, still exist. For example, the two routes as highlighted in Fig. 3.1(b) resemble two possible current paths supporting the second-order mode (TM_{21}). This means that the mesh geometry in Fig. 3.1(a), although designed for the fundamental mode (TM_{11}), can still excite higher-order modes to some extent.

Therefore, the design philosophy of the harmonics suppressing meshed circular patch

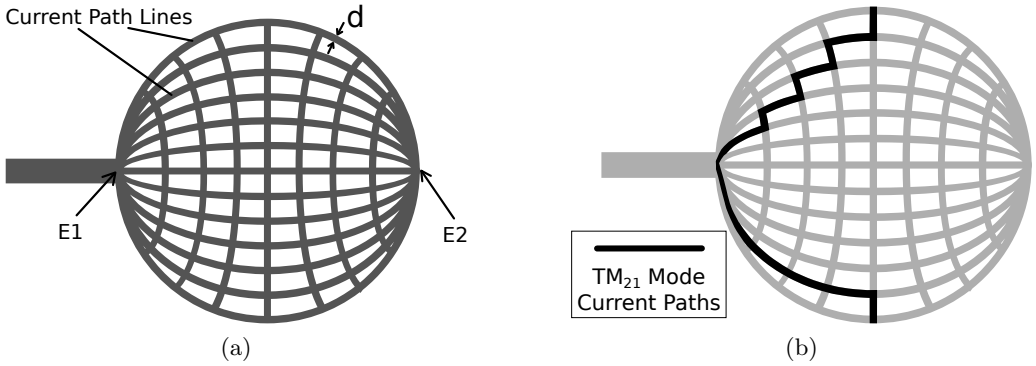

Fig. 3.1: Circular meshed patch antenna for fundamental mode: a) antenna geometry; b) antenna geometry with highlighted 2nd mode current paths.

antenna is such that it maintains the lines from E1 to E2, and then the other set of lines are carefully designed so that there is the minimum current paths for higher modes. By testing various geometries, it is found that the mesh geometry in Fig. 3.2 is the most effective in shifting the locations of the antenna's higher modes in the frequency domain. The reason is clear. In order to complete a patch geometry and to connect the current paths of the fundamental mode, only one orthogonal line (the center line) has been remained. At the meantime, by keeping the orthogonal line minimal and at the center, one reduces the possibilities of shaping current paths for higher modes. This geometry suppresses the second mode; and it gives an even stronger suppression to the third mode as the current paths for the third mode is very difficult to form with such a mesh geometry.

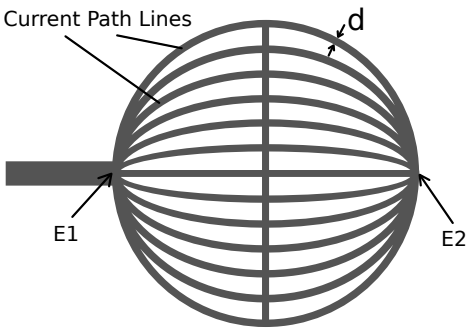

Fig. 3.2: Circular meshed patch antenna with harmonic suppression functionality.

3.2.2 Harmonic Suppression Capability

The measure for a successful harmonic suppression is the input impedance of the antenna, and it should be purely reactive at harmonics so that the PAE of the amplifier can be maximized [8]. Although most applications for the meshed antennas may need transparent dielectric as the substrate, the design philosophy of the harmonics suppressing meshed antennas is the same for the transparent and opaque substrates. Therefore, in the current laboratory validation, Roger's RO4003C laminate ($\epsilon_r = 3.55$, h = 1.524 mm, tanδ= 0.0021) was chosen to examine the design. The ground of the antenna is solid metal (not meshed). The meshed antenna as illustrated in Fig. 3.2 has a radius of 21 mm and a line-width (d in Fig. 3.2) of 1 mm.

The antenna geometry in Fig. 3.2 was simulated with Ansys's High Frequency Structure Simulator (HFSS) and prototyped as shown in Fig. 3.3. The simulated antenna's input impedance versus frequency is plotted in Fig. 3.4(a). The fundamental resonance is at 2.17 GHz, and it is seen that the antenna's input impedance at the second and third harmonics are almost purely reactive. In other words, the real parts of the impedance at those two frequencies are very small (less than 2.5Ω). This indicates that the radiation resistance at the harmonics is greatly suppressed. The real parts at those two harmonics are not zero (2.18Ω and 1.92Ω for the second and third harmonics) to be ideal, but this is primarily due to the material loss. It is apparent that the PA's harmonics are away from the antenna's resonant modes, resulting in no extra power loss from being radiated (i.e. higher PAE). The measurement of the input impedance was performed using a vector network analyzer (Agilent VNA 8510C) with the Through-Reflect-Line (TRL) calibration and the result is presented in Fig. 3.4(b). It can be seen that the measurement agrees very well with the simulation.

3.2.3 Radiation Properties

To verify the radiation properties of the meshed antenna, the radiation pattern at the fundamental frequency was measured and presented in Fig. 3.5. In order to perform the gain measurement, the antenna shown in Fig. 3.3 was stub-matched to the 50Ω SMA

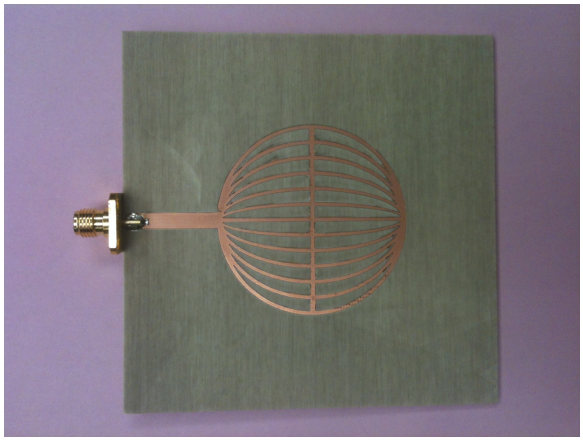

Fig. 3.3: Prototyped circular meshed patch antenna with harmonic suppression functionality.

connector using copper tape. It is seen that the patterns of both E- and H-plane resemble those of circular solid patch antennas. The maximum gain was measured to be close to 4 dB and the cross polarization level was -17 dB. The relatively low gain (compared to a 7-dB gain of a normal circular solid patch antenna) is mainly due to the meshing [2] but it can be improved to some extent by refining the mesh lines [4].

3.3 Substrate Effect on AIA Antenna Design

In order to investigate whether different substrates affect the harmonic suppression capability of the proposed meshed patch, the design on different dielectrics was examined. The design was tested on RT/Duroid 5870 (ϵ_r = 2.33, h = 0.74 mm, tanδ = 0.0012) through HFSS simulation and the input impedance versus frequency is plotted in Fig. 3.6, where the suppression of the second and third harmonics is obvious. The same circular meshed patch antenna was also tested on plexiglass, and similar simulation results were obtained. Therefore, it can be concluded that the proposed meshed antenna is not sensitive to substrates in terms of the harmonic suppression. This makes the meshed circular antenna a better design for AIA than the circular sector antenna developed by Radisic et al. [6–8]. In order to assist readers to see a clear comparison, the effect of substrates on that sector antenna is presented in the Appendix. It is seen that such a sector antenna's harmonic suppression capability depends on a careful choice of the substrate, and thus may cast

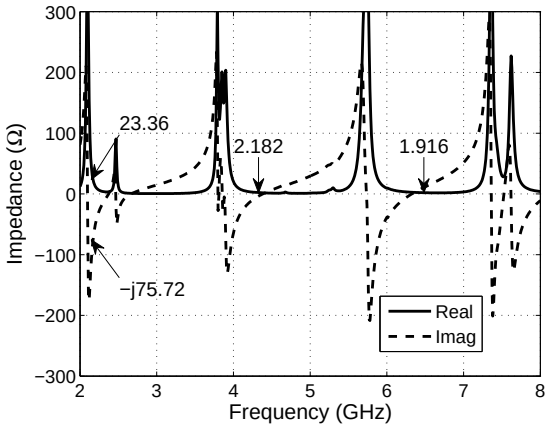

(a)

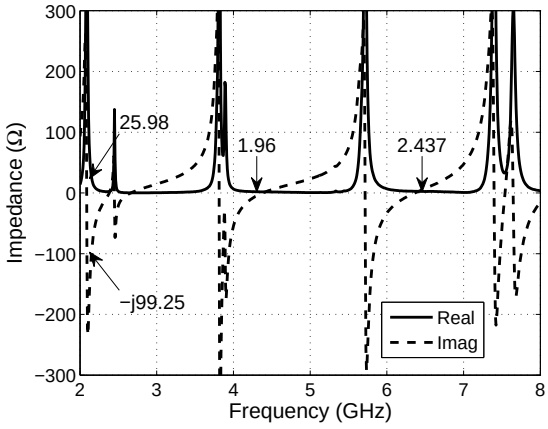

(b)

Fig. 3.4: Input impedance of the proposed circular meshed patch antenna on Roger's RO4003C: a) simulation; b) measurement.

challenges when the AIA needs to be performed on different dielectrics such as windshield or solar cells.

3.4 Conclusion

A circular meshed antenna with good harmonic turning capability has been presented. The antenna can be used in AIA design. The harmonic suppression capability of the proposed antenna has been validated through measurements and it has been shown that the design is not sensitive to different substrates as opposed to the reported circular sector antenna. In addition, since the meshed antenna design can be optically transparent and

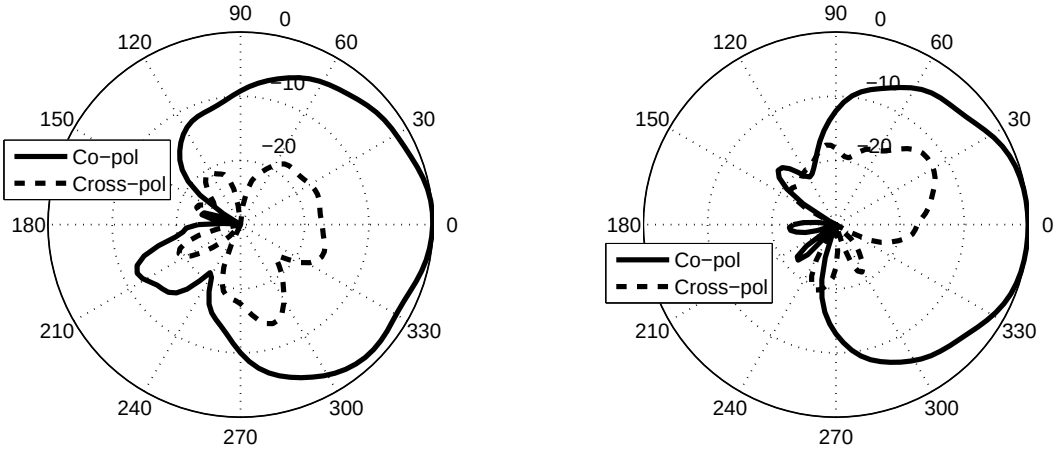

Fig. 3.5: Normalized radiation pattern of the proposed circular meshed patch antenna on Roger's RO4003C: a) E-plane; b) H-plane.

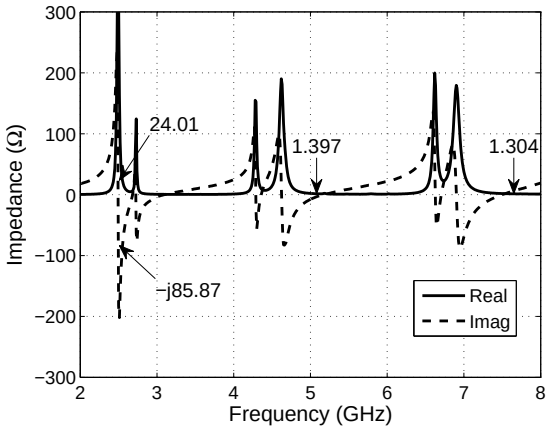

Fig. 3.6: Input impedance of the proposed circular meshed patch antenna on Roger's RT/Duroid 5870.

contain less metal than the classic patch antennas, the proposed antenna can be conveniently integrated on solar cells or vehicle windshield.

3.5 Appendix

The geometry of the circular solid sector designed by Radisic et al., as depicted in Fig. 3.7, was reported to effectively suppress the 2nd and 3rd harmonics [6–8]. In order to confirm

the validity of the design, the simulation with HFSS was repeated using the same RT/Duroid 5870 substrate (ϵ_rr = 2.33, h = 0.74 mm, tanδ = 0.0012) and the same antenna configuration as given in the original report [7]. Figure 3.8 shows the simulated input impedance against frequency, which agrees almost perfectly with the reported measurements [7].

When such a circular sector with a radius of 18 mm is designed on RO4003C substrate (ϵ_r = 3.55, h = 1.524 mm, tanδ = 0.0021), it can be found from both simulation and measurement that the harmonic suppression becomes bad. The input impedance of the antenna has large real parts for the second and especially the third harmonics (Fig. 3.9). And it can also be observed that the higher harmonics are located near resonances , indicating bad harmonic suppression. Since the discussed sector performs more poorly on RO4003C than on RT/Duroid 5870, it can be concluded that the harmonic suppression performance of this antenna configuration is subject to substrate parameters.

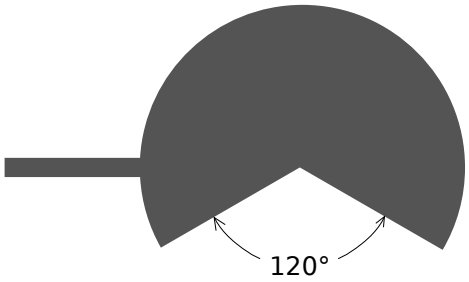

Fig. 3.7: Geometry of the circular sector patch antenna.

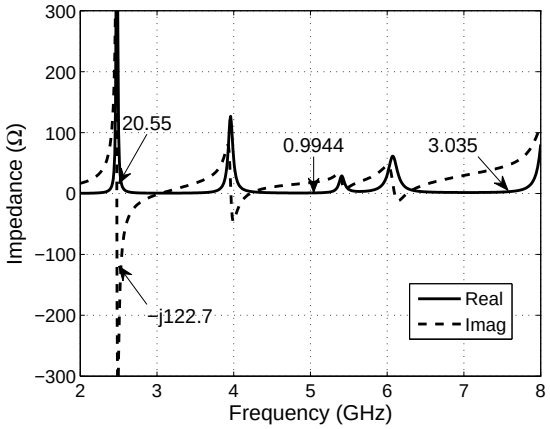

Fig. 3.8: Input impedance of the circular sector patch antenna on Roger's RT/Duroid 5870.

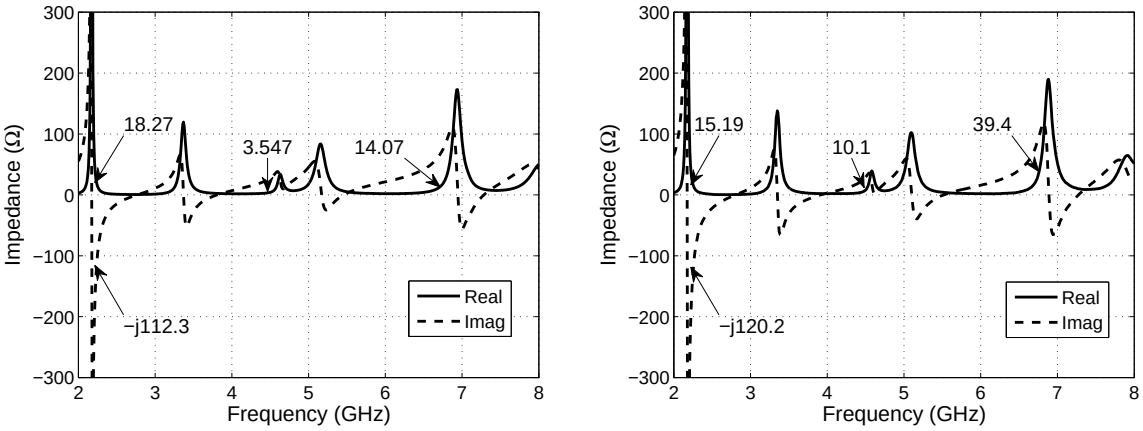

Fig. 3.9: Input impedance of the circular sector patch antenna on Roger's RO4003C: a) simulation; b) measurement.

References

[1] G. Clasen and R. Langley, "Meshed patch antennas," *IEEE Transactions on Antennas and Propagation*, vol. 52, no. 6, pp. 1412–1416, 2004.

[2] ——, "Meshed patch antenna integrated into car windscreen," *Electronics Letters*, vol. 36, no. 9, pp. 781–782, 2000.

[3] T. Turpin and R. Baktur, "Meshed patch antennas integrated on solar cells," *IEEE Antennas and Wireless Propagation Letters*, vol. 8, pp. 693–696, 2009.

[4] T. W. Turpin, "Meshed patch antennas integrated on solar cell - a feasibility study and optimization," Master's thesis, Utah State University, Logan, UT, 2009.

[5] T. Itoh, "Active integrated antennas for wireless applications," *Proceedings of Microwave Conference Asia-Pacific*, vol. 1, pp. 309–312, 1997.

[6] V. Radisic, Y. Qian, and T. Itoh, "Active antenna approach to high efficiency power amplifiers with EMI reduction," *Proceedings of IEEE Military Communications Conference*, vol. 3, pp. 699–703, 1998.

[7] ——, "Class F power amplifier integrated with circular sector microstrip antenna," *IEEE MTT-S International Microwave Symposium Digest*, vol. 2, pp. 687–690, 1997.

[8] ——, "Novel architectures for high-efficiency amplifiers for wireless applications," *IEEE Transactions on Microwave Theory and Techniques*, vol. 46, no. 11, pp. 1901–1909, 1998.

[9] ——, "Broadband power amplifier integrated with slot antenna and novel harmonic tuning structure," *IEEE MTT-S International Microwave Symposium Digest*, vol. 3, pp. 1895–1898, 1998.

[10] V. Radisic, S. T. Chew, Y. Qian, and T. Itoh, "High-efficiency power amplifier integrated with antenna," *IEEE Microwave and Guided Wave Letters*, vol. 7, no. 2, pp. 39–41, 1997.

[11] K. Chang, R. York, P. Hall, and T. Itoh, "Active integrated antennas," *IEEE Transactions on Microwave Theory and Techniques*, vol. 50, no. 3, pp. 937–944, 2002.

[12] S.-Y. Lin, K.-C. Huang, and J.-S. Chen, "Harmonic control for an integrated microstrip antenna with loaded transmission line," *Microwave and Optical Technology Letters*, vol. 44, no. 4, pp. 379–383, 2005.

[13] Y. Sung, M. Kim, and Y. Kim, "Harmonics reduction with defected ground structure for a microstrip patch antenna," *IEEE Antennas and Wireless Propagation Letters*, vol. 2, no. 1, pp. 111–113, 2003.

[14] P. Colantonio, F. Giannini, E. Limiti, and G. Marrocco, "A method for PA-patch antenna design optimization oriented to maximum efficiency," *12th GAAS Symposium*, pp. 25–28, 2004.

[15] S. Kwon, B. M. Lee, Y. J. Yoon, W. Y. Song, and J.-G. Yook, "A harmonic suppression antenna for an active integrated antenna," *IEEE Microwave and Wireless Components Letters*, vol. 13, no. 2, pp. 54–56, 2003.

Chapter 4

Circularly Polarized Meshed Patch Antenna for Small Satellite Application

Abstract

A circularly polarized meshed patch antenna design is presented. The proposed antenna consists of two square meshed patches, which generate two orthogonal linear polarizations at two slightly different frequencies. A common proximity feed line is utilized to excite the two patches and a 90^{o} phase difference can be achieved between the two resonant frequencies, which is needed for circular polarization. The overall structure of this antenna is highly compatible with solar panels; thus, it is of great significance for small satellite applications. The measured results of the antenna prototype show that it has a 3-dB axial ratio (AR) bandwidth of 15 MHz, a 10-dB impedance bandwidth of 2%, and a gain of 5.15 dB at its center frequency 2.47 GHz.

4.1 Introduction

One of the challenges of cube satellites (CubeSats), an emerging crucial tool for space exploration, is their limited surface area that imposes restrictions on amount of solar cells, positions of antennas and space instruments. Therefore, optically transparent antennas that can be integrated on top of solar cells are desirable potential solution for the limited real estate issue [1–3]. Although transparent conductor such as indium tin oxides (ITO) can be applied for transparent antenna design [2, 3], ITO antennas have been shown to have very low efficiency at lower frequencies (e.g. S-band) and the transparencies are too low for solar cell integration. On the other hand, meshed antennas can be designed with very high transparency (>93%) and good efficiency for S-band [1,3], where most CubeSat applications lie. When a meshed patch antenna is achieved with a circular polarization (CP), it will be

immune from the Faraday effect [4] in the earth's ionosphere, which makes it even more favorable for satellite applications.

CP for regular patch antennas can be generated by exciting two orthogonal patch modes with 90^{o} phase difference [5]. One common method to realize this is to apply two feeds in phase quadrature to two adjacent sides of a square patch [6]. Another typical technique is to design a square patch with a pair of truncated diagonal corners that is excited using a single feed [6]. For a meshed antenna, however, neither of these two methods is practical. While the dual-feed method is bulky and the feed lines would inevitably hinder the integration with solar cells, the method of corner truncation requires a very careful and low-tolerance design of mesh geometry to efficiently conduct the currents of complicated patterns to support the two resonant modes for a CP. Similarly, due to either complex mesh design or inappropriate feed structure, many other available techniques [7–11] to achieve circular polarization are not suitable for solar cell and meshed patch integration.

This paper presents a circularly polarized meshed antenna composed of two meshed patch elements that are coupled with a single feed line. Because the non-transparent feed line can be placed along the gaps (G in Fig. 4.1(a)) between solar cells, the design is highly compatible with solar panels of small satellites such as a CubeSat (Fig. 4.1(a)). The meshed patches, which are highly transparent to the solar light, can be placed on top of solar cells. The performances of the proposed antenna were verified by the measurement results, such as return loss, radiation pattern and axial ratio (AR).

4.2 Antenna Design

The typical assembly of a surface-mounted solar panel on a CubeSat is schematically displayed in Fig. 4.1(b), where the solar cells are mounted on the conductive shielding of the satellite and covered with a layer of cover glass in order to protect the solar cells. In our design, the cover glass acts as the dielectric substrate for the transparent meshed antennas, and the metallic shielding is used as the ground. The antenna's loss due to the active junctions of solar cells is not the objective of this paper as it has been experimented previously [12]. The effect of the earth on the antenna, as well as the noise temperature, is

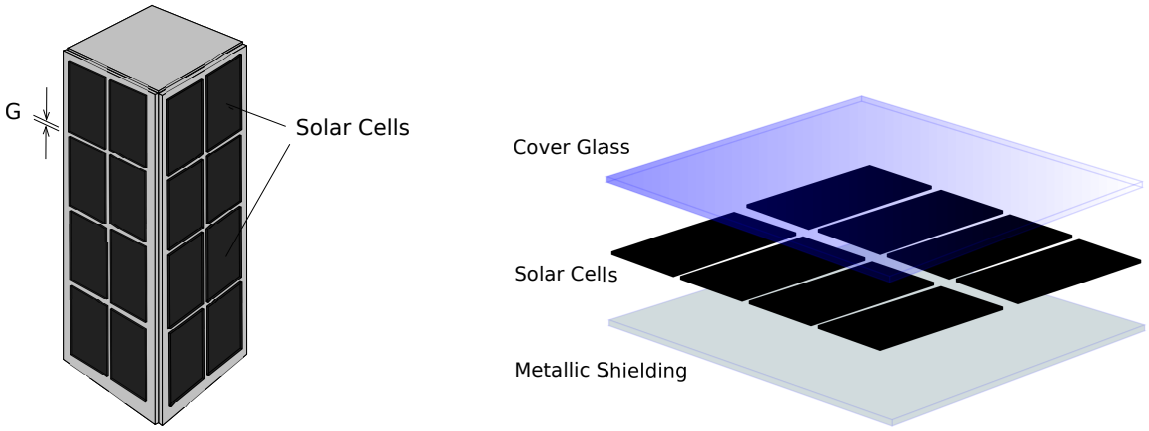

(a) (b)

Fig. 4.1: Solar panel on a CubeSat: a) isometric view of a CubeSat; b) typical structure of the solar panel.

not discussed either because the first issue is not prominent for a CubeSat communication link budget and the second issue is considered simply by using the sky's temperature [1].

4.2.1 Capacitive and Inductive Proximity-Fed Square Patch

The basis of the proposed design is a coplanar proximity from previous studies [13, 14], where the feed is an open-ended microstrip line. There are two different coupling mechanisms for this type of feeding technique: capacitive and inductive coupling. As an example, a square patch with the capacitive coupling is depicted in Fig. 4.2(a), where the central line of the patch is aligned at a half wavelength from the tip (T) of the open ended feed line. In this configuration, the voltage standing wave on the feed line has a magnitude maximum that coincides at the patch center and, through coupling across the gap, excites a fundamental resonant current pattern (illustrated with arrows in Fig. 4.2(a)) in the direction perpendicular to the feed line, indicating a linearly polarized radiation in the far field. In the case of inductive coupling (Fig. 4.2(b)), the edge of the square patch is aligned with the tip of the feed line. The patch is driven by the magnitude maximum of the current standing wave, which is 90^{o} out of phase with the voltage standing wave. The surface current and the radiation polarization of this patch are both orthogonal to their

counterparts from the capacitive coupling case.

The two proximity feed methods in Fig. 4.2 can be applied to meshed square patches as shown in Fig. 4.3. The number of current carrier lines (the ones providing paths for the resonant currents) of the meshed patch can be made higher than that of equipotential lines (the ones only responsible for cross-connecting current carrier lines) in an attempt to promote the desired polarization while suppressing the cross-polarization level of the antenna.

4.2.2 Circular Polarization Design

A CP can be decomposed into two linear polarizations that are orthogonal in space and quadrature in phase. The two meshed patch antennas, displayed in Fig. 4.3, radiate two linear polarizations orthogonal to each other. By combining these two antennas into a more

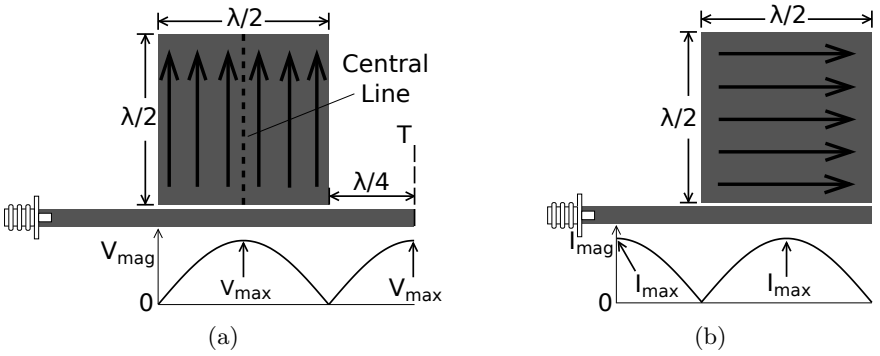

Fig. 4.2: Coupling mechanisms of coplanar proximity feed: a) capacitive coupling; b) inductive coupling.

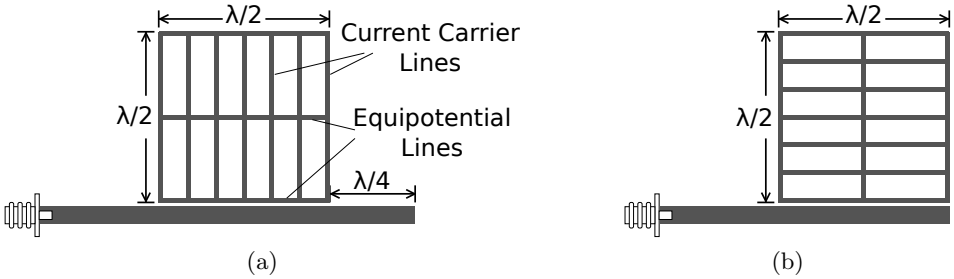

Fig. 4.3: Coupling mechanisms of coplanar proximity feed: a) capacitive coupling; b) inductive coupling.

compact configuration without changing their polarization directions, the proposed meshed antenna for circular polarization, as shown in Fig. 4.4, can be achieved provided that the two element patches resonate at slightly different frequencies. The reason for having two very close but not the same frequency is explained in the following paragraph.

The common feed line in this design is able to provide the two patches with the two types of coupling methods described earlier in II-A. In the instant the increasing voltage magnitude and decreasing current magnitude, as conceptually illustrated in Fig. 4.5, are formed along the open ended feed line, the current on the feed line induces decreasing currents, through inductive coupling, on the patch below the feed line (illustrated with black arrows in Fig. 4.5). At the same time, the voltage on the feed line creates the decreasing surface currents, via capacitive coupling, flowing from the gap side towards the opposite end of the other patch (illustrated with black arrows in Fig. 4.5). Thus, the currents on the two patches appear in phase if the two patches resonate at the same frequency. Therefore, the two patches should be designed to resonate at two slightly different frequencies.

Therefore, one can achieve a CP from the antenna configuration, illustrated in Fig. 4.4, by carefully adjusting the sizes of the two patches such that the difference between their resonant frequencies results in a required 90^{o} phase difference [5]. For the configuration in Fig. 4.4, a left-handed circular polarization (LHCP) can be achieved by having the capacitively coupled patch resonate at a higher frequency, whereas having the inductively

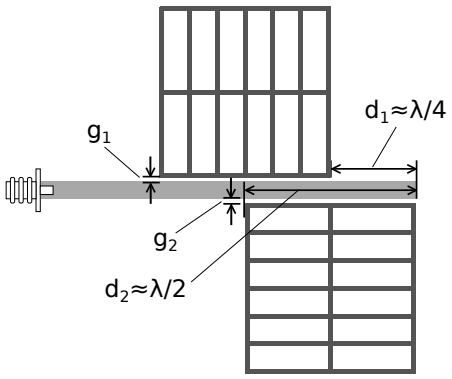

Fig. 4.4: Meshed patch antenna for circular polarization.

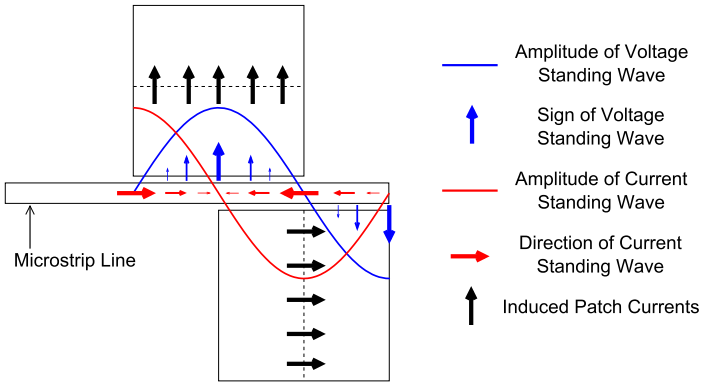

Fig. 4.5: Mechanism details of a CP meshed antenna

coupled patch resonate at a higher frequency yields a right-handed circular polarization (RHCP).

4.3 Results and Discussion

Although in the actual implementation of integration with solar cells, a transparent dielectric (e.g. cover glass) will be the substrate for meshed patch antennas, the design philosophy of the CP meshed antennas is the same for transparent and non-transparent substrates. Therefore, in the current laboratory validation, Roger's RO4003C laminate (ϵ_r = 3.55, h = 1.524 mm, tanδ = 0.0021) was chosen to examine the design. The two meshed patches are transparent to lights and the transparency is defined as the ratio of the see-through area over the entire patch area. The meshed patches can be placed on solar cells whereas the non-transparent feed line can be placed along the gap between solar cells (G in Fig. 4.1(a)). The transparency of the meshed antenna can be controlled by the width and the number of the mesh lines. The relation between the transparency and antenna properties has been found by Turpin [15]. The operational frequency is chosen to be in S band, where the size of the meshed patch is realistic to be placed on top of a commercial triple-junction solar cells used in space applications.

The prototyped antenna was designed using ANSYS's High Frequency Structure Simulator (HFSS). In order to have the right frequency shift between the resonant frequencies,

the patch sizes of this antenna need to be carefully designed. While all the mesh lines were set to be 1 mm wide, the capacitively coupled meshed patch was designed to be 30 mm $\times$ 30 mm and the inductively coupled meshed patch was set to 30.5 mm $\times$ 30.5 mm. This generates an LHCP. The impedance matching was obtained by tuning the design parameters: the gaps (g_1 and g_2 in Fig. 4.4) between the patches and the 50Ω feed line; and the distances of the patches from the tip of the feed line (d_1 and d_2 in Fig. 4.4).

An RHCP can be designed from the method explained in II-B. Or one can simply flip the LHCP configuration to obtain an RHCP antenna as shown in Fig. 4.6.

The prototyped LHCP antenna is shown in Fig. 4.7. It has a transparency of 70% and was fabricated with a circuit board milling machine. The lower transparency was chosen for the ease of fabrication. The LHCP meshed antenna was measured using an Agilent's VNA 8510C and NSI near-field antenna range in an anechoic chamber. The measured S_{11} parameter in comparison with its HFSS simulated result is presented in Fig. 4.8. It is seen that the two curves almost overlap with each other. The 10-dB impedance bandwidth is about 2%, a typical value for patch antennas. Figure 4.9 presents the variation of the antenna's AR with frequency, both the simulation and measurement, in the normal direction of the antenna (Z in Fig. 4.7). It can be seen that the minimum AR (1.3 dB) appears at 2.48 GHz in the simulation and at 2.47 GHz in the measurement, which is a very good agreement. The 3-dB AR bandwidth is about 15 MHz (2.461 GHz to 2.476 GHz) in the

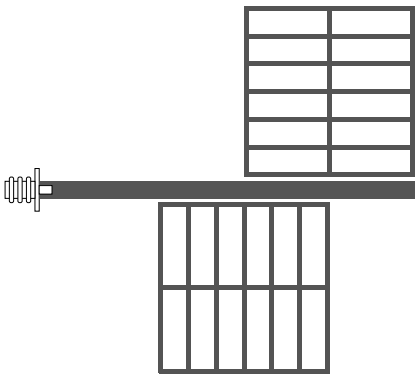

Fig. 4.6: Geometry of an RHCP meshed antenna.

measurement, which falls into the 10-dB impedance bandwidth range (Fig. 4.8). This results indicate that the antenna can function efficiently with a good AR.

The orientation of the antenna under test with respect to the cartesian coordinate system is illustrated in Fig. 4.7. The variations of the antenna's AR with respect to θ and ϕ at 2.47 GHz were measured and plotted in Fig. 4.10, where the 3-dB AR beamwidth is about 20^o on the plane of $\phi = 0^o$ and about 80^o on the $\phi = 90^o$ plane. This can also be observed from the measured radiation patterns for the minimum AR, which are plotted in Fig. 4.11. These AR beamwidth values are sufficient for a CubeSate link budget. It can also be seen from Fig. 4.11 that the measured radiation pattern agrees well with the simulation, and the cross polarization level is below -22 dB in the broadside direction at the center frequency. The gain of the antenna was measured to be 5.15 dB at the center frequency 2.47 GHz. Also, this measured gain agrees very well with the simulation of 5.96 dB.

4.4 Conclusion

In this paper, a design of an optically transparent antenna with circular polarization has been presented after a detailed study of a coplanar proximity feed scheme. The design is suitable for small satellite applications as it can be conveniently integrated with solar panels of small satellites to save surface real estate. The proposed antenna consists of two square

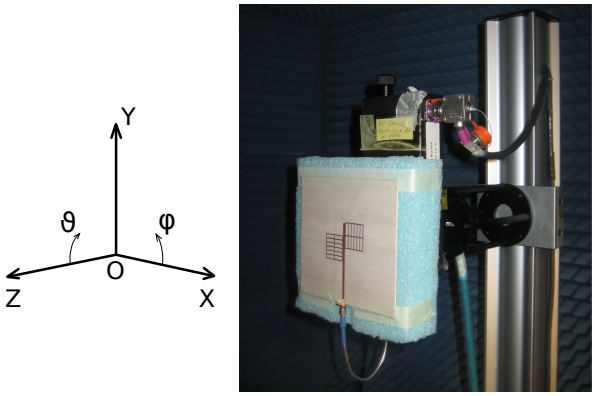

Fig. 4.7: Prototype of LHCP meshed antenna under test.

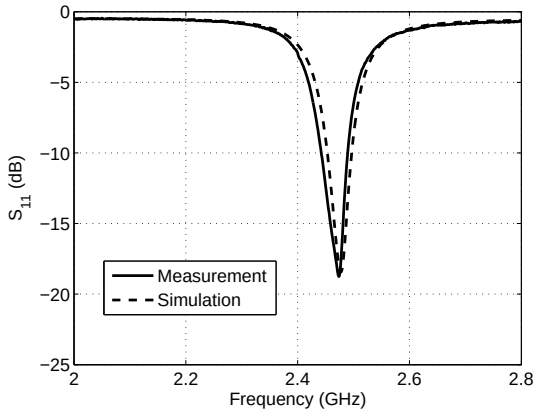

Fig. 4.8: S_{11} of LHCP meshed antenna.

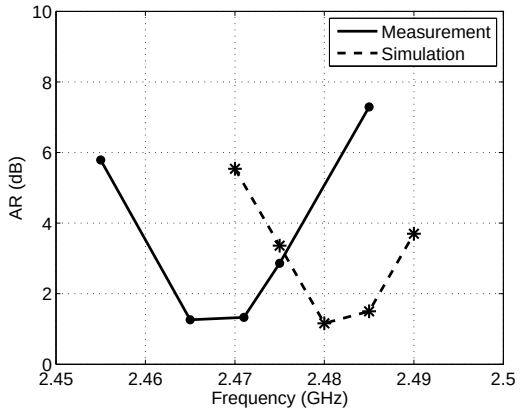

Fig. 4.9: AR of LHCP meshed antenna vs. frequency in the normal direction.

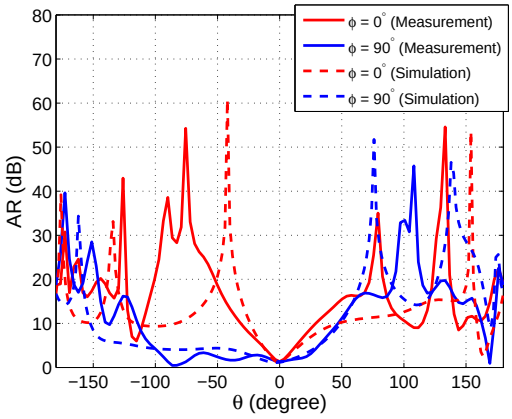

Fig. 4.10: Spatial AR of LHCP meshed antenna.

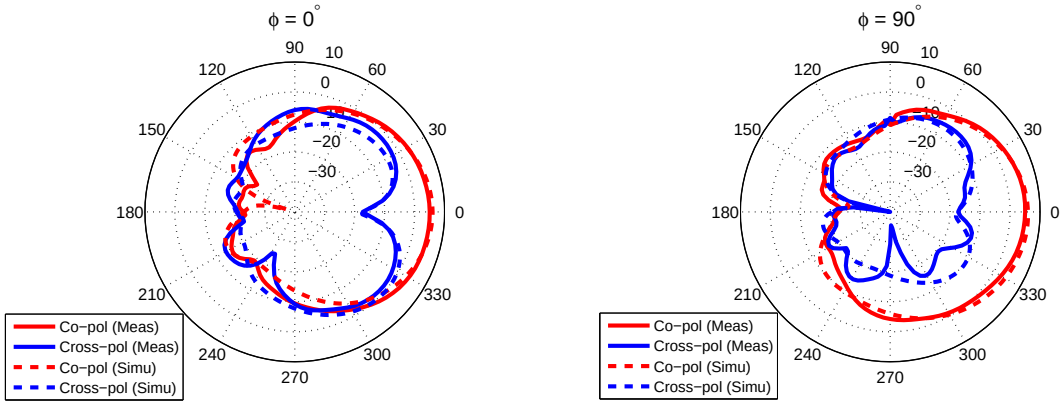

(a) (b)

Fig. 4.11: Radiation of LHCP meshed antenna: a) $\phi = 0^{o}$ plane; b) $\phi = 90^{o}$ plane.

meshed patches fed with a straight microstrip line, which generates two linear polarizations that are orthogonal in space and quadrature in phase, leading to a circular polarization. The measured AR is reasonable and lies within the bandwidth of the resonant frequency. The measured cross polarization level is below -22 dB in the normal direction. The realized gain is more than 5 dB, which is reasonable because there is some loss due to meshing [15].

The proposed antenna design was validated at a transparency of 70% on a non-transparent circuit board substrate. But the transparency of the meshed antenna can be increased by refining the mesh lines and the same design method can be used to produce CP meshed antennas on the cover glass of solar cells.

There may be some challenges when prototyping this antenna because a good CP depends on the coupling of the patches with the feed line, which is sensitive to the coupling gaps. However, a careful fabrication with a regular circuit board milling machine can still yield a satisfactory result. Therefore, further refining mesh lines [15] with a more accurate manufacturing process is beneficial in achieving an optimal transparent, efficient antenna with a good CP character.

References

[1] T. Turpin and R. Baktur, "Meshed patch antennas integrated on solar cells," *IEEE Antennas and Wireless Propagation Letters*, vol. 8, pp. 693–696, 2009.

[2] T. Yasin, R. Baktur, and C. Furse, "A study on the efficiency of transparent patch antennas designed from conductive oxide films," *Proceedings of IEEE International Symposium on Antennas and Propagation*, pp. 3085–3087, 2011.

[3] ——, "A comparative study on two types of transparent patch antennas," *Proceedings of XXXth URSI General Assembly and Scientific Symposium*, pp. 1–4, 2011.

[4] R. C. Johnson and H. Jasik, *Antenna Engineering Handbook*. New York: McGraw-Hill, 1984.

[5] D. M. Pozar and D. H. Schaubert, *Microstrip Antennas: The Analysis and Design of Microstrip Antennas and Arrays*. New York: IEEE Press, 1995.

[6] J. R. James and P. S. Hall, *Handbook of Microstrip Antennas*. London: Peter Peregrinus Ltd, 1989.

[7] W.-S. Chen, C.-K. Wu, and K.-L. Wong, "Novel compact circularly polarized square microstrip antenna," *IEEE Transactions on Antennas and Propagation*, vol. 49, no. 3, pp. 340–342, 2001.

[8] J.-S. Row and C.-Y. Ai, "Compact design of single-feed circularly polarised microstrip antenna," *Electronics Letters*, vol. 40, no. 18, pp. 1093–1094, 2004.

[9] T. Sudha, T. Vedavathy, and N. Bhat, "Wideband single-fed circularly polarised patch antenna," *Electronics Letters*, vol. 40, no. 11, pp. 648–649, 2004.

[10] C. Ravipati and L. Shafai, "A wide bandwidth circularly polarized microstrip antenna using a single feed," *IEEE Antennas and Propagation Society International Symposium*, vol. 1, pp. 244–247, 1999.

[11] T.-W. Li, C.-L. Lai, and J.-S. Sun, "Study of dual-band circularly polarized microstrip antenna," *The European Conference on Wireless Technology*, pp. 79–80, 2005.

[12] J. A. Arellano, "Inkjet-printed highly transparent solar cell antennas," Master's thesis, Utah State University, Logan, UT, 2011.

[13] T. Miyazaki and K. Itoh, "Analysis and design on a proximity fed microstrip antenna," *Proceedings of the International Symposium on Antennas and Propagation Japan*, vol. 2, pp. 545–548, 1996.

[14] J. Saberin, "Optically transparent antennas for small satelllites," Master's thesis, University of Utah, Salt Lake City, UT, 2010.

[15] T. W. Turpin, "Meshed patch antennas integrated on solar cell - a feasibility study and optimization," Master's thesis, Utah State University, Logan, UT, 2009.

Chapter 5

Circularly Polarized Meshed Patch Antenna Using Coplanar Y-Shaped Coupling Feed

Abstract

This letter describes a circularly polarized optically transparent meshed patch antenna designed for small satellite applications. The antenna consists of a nearly square meshed patch that is fed with a coplanar Y-shaped feed. The configuration of the antenna and feed network has the advantage of being integrable with solar panels of small satellites to resolve the limited surface area issue. The results for a prototyped left-handed circularly polarized antenna operating at 2.34 GHz are presented. The axial ratio is 2 dB, and the gain is 4.7 dB at the center frequency. The 10-dB impedance bandwidth is close to 2% and the 3-dB axial ratio bandwidth is 7 MHz.

5.1 Introduction

Meshed patch antennas with optical transparency can be built on clear substrates such as the car windshield [1–3]. They can also be integrated with the solar panels on small satellites (e.g. cube satellites or CubeSats) [4], which are becoming popular vehicles for space exploration. These antennas, when designed to have circular polarization (CP), will be able to alleviate the Faraday rotation effect in the earth's ionosphere [5]. It is straightforward to obtain a CP by exciting two orthogonal resonant modes with 90^{o} phase difference on a square, rectangular or circular microstrip patch [6, 7]. But most of these techniques either use a feed structure too complex for solar panel integration or involve certain modification of the patch element in order to alter the current paths. This letter presents a very simple circularly polarized meshed antenna design that can be easily integrated with solar panels. The antenna is of left-handed circular polarization (LHCP) and has an optical transparency

of 60%. But the transparency can be conveniently improved to a level of higher than 90%, using the optimization method reported by Turpin [8], to facilitate direct integration of the antenna with solar cells.

5.2 Antenna and Feed Network

A typical assembly of the solar panel on a CubeSat is illustrated in Fig. 5.1, where the solar cells are mounted on the conductive shielding of the satellite and covered with a protection layer of cover glass. There are usually gaps between solar cells for either electric connection or thermal expansion. The potential application of the proposed transparent meshed patch antenna is to integrate it directly on top of the cover glass to save surface real estate. The cover glass will act as the dielectric substrate, and the metallic shielding together with the solar cells will be the ground plane. The antenna loss due to the active solar cell junctions is not the objective of this paper as it has been experimentally studied [9]. The effect of the earth on the antenna as well as the noise temperature are not discussed either because the first issue is not prominent for the CubeSat communication and the second issue is considered in the link budget simply by using the sky's temperature [4].

The basic geometry of the proposed CP meshed patch antenna is shown in Fig. 5.2. The side lengths of the patch are slightly different ($d_1 \neq d_2$ in Fig. 5.2) in order to achieve two orthogonal resonant modes with 90° phase difference [6]. When d_1 is greater than d_2, it can generate an LHCP. For a right-handed circular polarization (RHCP), d_1 needs to be smaller than d_2. These two modes are excited using a non-transparent Y-shaped coupling

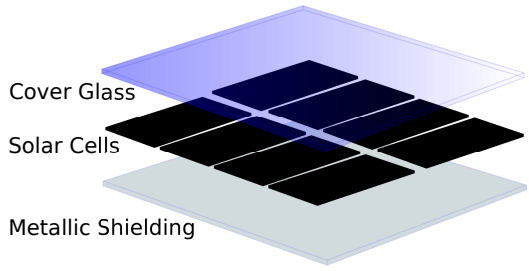

Fig. 5.1: Typical assembly of solar panels on small satellites.

feedline, which also acts as the impedance matching network between the meshed patch and the source. The thicker part of the feedline can be placed along the gaps between the solar cells such that it does not block the solar cells from the solar light. The lengths of the two branches of the Y-shaped feedline are extended to the centers of the respective sides of the patch. This is chosen such that the coupling lines are long enough to drive the antenna but not too long to cast too much shadow onto the solar cells underneath. In this design, the branch width (t in Fig. 5.2) and the gap (g in Fig. 5.2) between the patch and feed are the two tuning parameters for impedance matching.

5.3 Results and Discussion

Although the actual implementation of the solar cell integrated meshed patch antenna needs transparent dielectric (i.e. cover glass) as the substrate, the design philosophy of achieving CP is the same for transparent and non-transparent substrates. Therefore, in the laboratory validation of this study, Roger's RO4003C laminate ($\epsilon_r = 3.55$, h = 1.524 mm, tan$\delta = 0.0021$) was chosen to examine the design.

An LHCP meshed patch antenna of the structure shown in Fig. 5.2 was designed using ANSYS's High Frequency Structure Simulator (HFSS). The dimensions of the meshed patch are $d_1 = 30.6$ mm and $d_2 = 30$ mm, and the uniform width of all the mesh lines of the patch is 1 mm. This yields an optical transparency of 60% within the patch area. The relatively low transparency with thicker mesh lines was chosen mainly for easy prototyping. However,

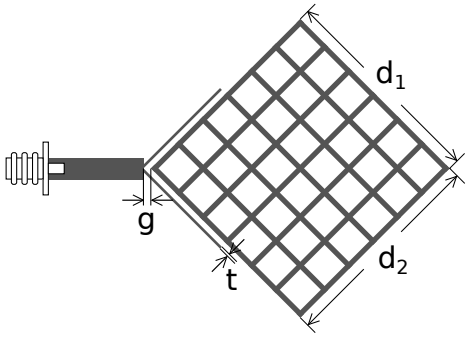

Fig. 5.2: Geometry of proposed CP meshed patch antenna.

a higher transparency (> 90%) can be conveniently achieved by refining the mesh lines [8]. The gap and the feedline branch thickness (g and t in Fig. 5.2) were found to be 1.2 mm and 0.5 mm, respectively, for a good impedance match (S_{11} < -20 dB).

The antenna was prototyped with a circuit board milling machine (Fig. 5.3) and measured using Agilent's VNA 8510C and NSI near-field antenna range in the anechoic chamber. The measured S_{11} in comparison with the simulation result is presented in Fig. 5.4, where they agree with each other very well. The 10-dB impedance bandwidth is approximately 2%, a typical value for microstrip patch antennas.

The orientation of the antenna under test with respect to the Cartesian coordinate

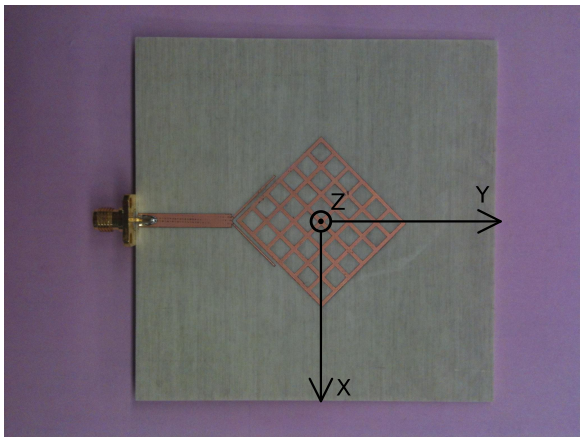

Fig. 5.3: Prototype of LHCP antenna with coordinate system indicated.

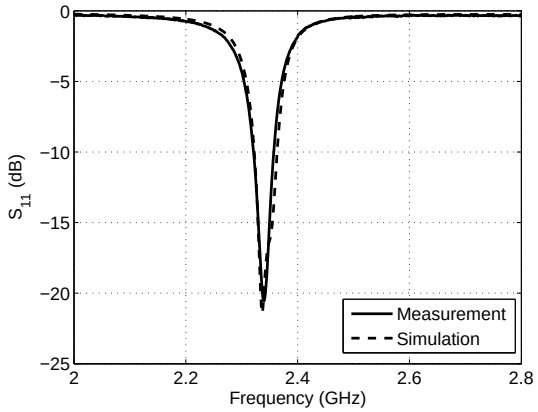

Fig. 5.4: S_{11} of LHCP meshed patch antenna.

system is illustrated in Fig. 5.3. The variations of the antenna's axial ratio (AR) with respect to θ and ϕ at the center frequency (2.34 GHz) were measured and plotted in Fig. 5.5, where the 3-dB AR beamwidth is about 100° on the plane of $\phi = 0°$ and about 60° on the $\phi = 90°$ plane. The AR value in the normal direction ($\theta = 0°$) is 1.7 dB in the simulation and 2.0 dB in the measurement. The measured 3-dB AR bandwidth is 7 MHz, which entirely falls into the 10-dB impedance bandwidth range, indicating that the antenna can function efficiently with a good AR.

Figures 5.6 and 5.7 show the radiation patterns of the proposed antenna at the center frequency (2.34 GHz), where the simulation and measurement results agree with each other quite well. It can be seen that the cross polarization level is below -20 dB in the broadside direction. The measured gain of the antenna is 4.7 dB, and it agrees well with the simulation result of 5.4 dB.

5.4 Conclusion

An LHCP meshed patch antenna design has been reported. Results are presented that demonstrate a good axial ratio, a low return loss and a decent gain. The optical transparency of the patch can be further improved by refining the mesh lines. The coplanar Y-shaped coupling feed network with two tuning parameters works effectively, and this

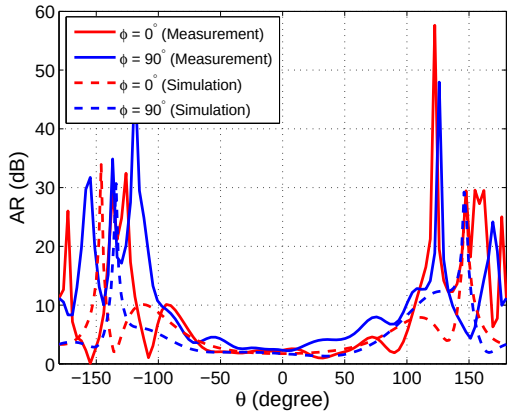

Fig. 5.5: Spatial AR of LHCP meshed patch antenna at center frequency.

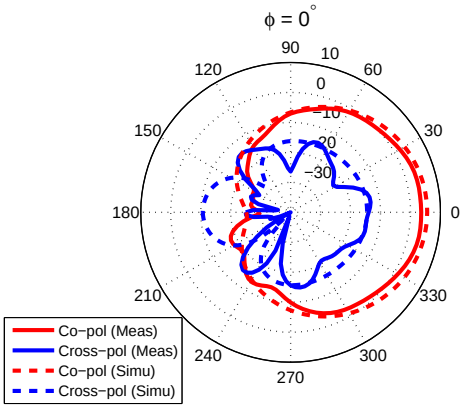

Fig. 5.6: Gain pattern of LHCP meshed patch antenna on $\phi = 0^o$ plane at center frequency.

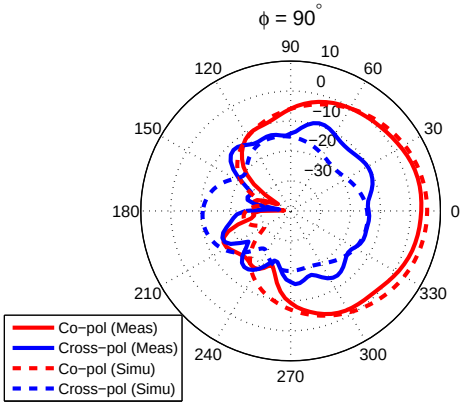

Fig. 5.7: Gain pattern of LHCP meshed patch antenna on $\phi = 90^o$ plane at center frequency.

simple design enables a potential integration with solar panels.

References

[1] K. Ito and M. Wu, "See-through microstrip antennas constructed on a transparent substrate," *7th IET International Conference on Antennas and Propagation*, pp. 133–136, 1991.

[2] G. Clasen and R. Langley, "Meshed patch antenna integrated into car windscreen," *Electronics Letters*, vol. 36, no. 9, pp. 781–782, 2000.

[3] ——, "Meshed patch antennas," *IEEE Transactions on Antennas and Propagation*, vol. 52, no. 6, pp. 1412–1416, 2004.

[4] T. Turpin and R. Baktur, "Meshed patch antennas integrated on solar cells," *IEEE Antennas and Wireless Propagation Letters*, vol. 8, pp. 693–696, 2009.

[5] R. C. Johnson and H. Jasik, *Antenna Engineering Handbook*. New York: McGraw-Hill, 1984.

[6] D. M. Pozar and D. H. Schaubert, *Microstrip Antennas: The Analysis and Design of Microstrip Antennas and Arrays*. New York: IEEE Press, 1995.

[7] P. Sharma and K. Gupta, "Analysis and optimized design of single feed circularly polarized microstrip antennas," *IEEE Transactions on Antennas and Propagation*, vol. 31, no. 6, pp. 949–955, 1983.

[8] T. W. Turpin, "Meshed patch antennas integrated on solar cell - a feasibility study and optimization," Master's thesis, Utah State University, Logan, UT, 2009.

[9] J. A. Arellano, "Inkjet-printed highly transparent solar cell antennas," Master's thesis, Utah State University, Logan, UT, 2011.

Chapter 6

Bandwidth-Enhanced Meshed Patch Antenna Design

Abstract

This paper presents an impedance bandwidth enhancement method for optically transparent meshed patch antennas using a coplanar proximity feed. The antenna design is highly compatible for integration with solar panels. The proposed antenna consists of three meshed patch elements with slightly different sizes, resulting in an improved impedance bandwidth that is approximately 2.5 times as wide as that of a single-element meshed patch antenna.

6.1 Introduction

Cube satellites (CubeSats) are emerging as crucial tools for space exploration. As a CubeSat has a very limited surface area, it is highly valuable to have antennas integrated with solar panels. One of such compatible designs is a highly transparent meshed antenna [1]. However, a meshed patch antenna, just as its solid counterpart, suffers from narrow impedance bandwidth, which is intrinsic to all microstrip patch antennas [2]. Also, most CubeSats use very simple communication systems and do not require high bandwidth, a wider bandwidth can be beneficial for extending CubeSat applications to areas where high data rate is essential. Therefore, it is important to explore methods that improves meshed antenna bandwidth.

There have been a wide variety of techniques proposed for improving the impedance bandwidth of conventional microstrip patch antennas. As concluded by Pozar and Schaubert [2], the majority of these methods can be categorized into three canonical approaches: first, by using a matching network [3]; second, by introducing multiple resonances [4]; and third, by introducing loss [5]. In recent years, other new methods for increasing bandwidth, such as adopting metamaterial concepts [6], have been reported. Most of these approaches may

not be applicable for meshed patch antennas integrated with solar panels due to their special properties. For example, introducing extra loss (e.g. by adding a resistive component [5]) is not favored since it decreases the efficiency of meshed patch antennas, which is already lower than that of regular patch antennas [7]. The metamaterial technique usually involves special patterns on both the patch and ground plane, but it is hard to design such patterns on the patch and to have high optical transparency.

In this paper, a bandwidth enhancement technique is proposed by utilizing multiple resonances. The design is compatible with solar cell integration. The experimental results show that the bandwidth of the proposed antenna is 2.5 times as wide as that of a single meshed patch element with the same feed configuration.

6.2 Antenna Structure

6.2.1 Coplanar Proximity Feed Structure

Figure 6.1 illustrates an isometric view of a CubeSat and its solar panel assembly. As seen, the solar panel of a small satellite consists of a conductive shielding (as part of the satellite's metallic box), solar arrays and a cover glass (dielectric). There are gaps (G in Fig. 6.1(a)) between the solar cells, and thus a regular microstrip line can be placed on top of the cover glass right above one of these gap lines. The microstrip line, even though not transparent, can be used to feed the meshed antennas without casting significant shadows on solar cells. Because of the specific structure of CubeSat solar panels and those gap lines, feeding techniques that employ only a straight microstrip line, such as the proximity coupling feed [8,9], are better suited for antenna-solar-cell integration. This type of feeding method is not only simple, but also can be extended to antenna arrays.

The basic building block of the proposed bandwidth enhancement method is as illustrated in Fig. 6.2, where a square patch antenna is proximity-fed by a straight microstrip line. The central line (marked with a dash line in Fig. 6.2) of the patch is aligned at half wavelength from the tip (T in Fig. 6.2) of the open-ended microstrip feed line. The voltage standing wave along the feed line has a maximum that coincides at the patch center and,

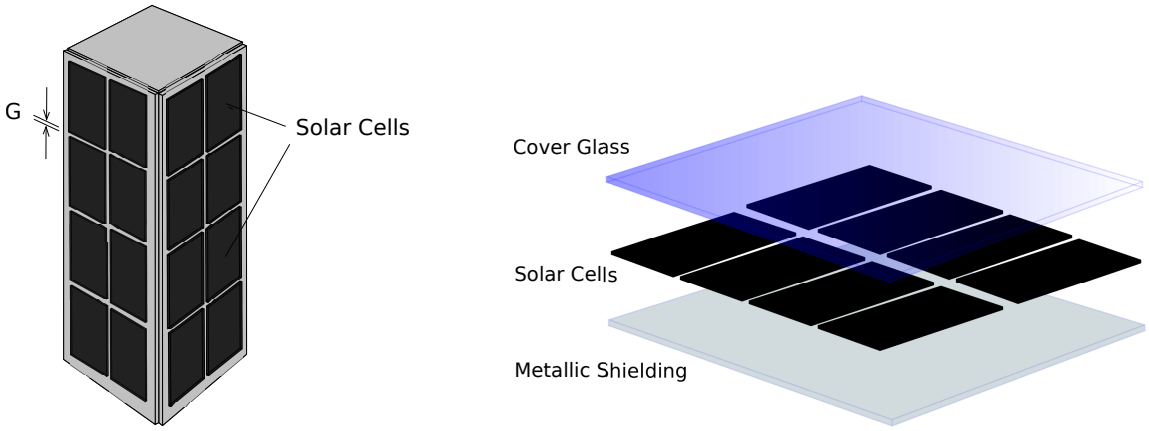

(a) (b)

Fig. 6.1: Solar panel of CubeSat: a) isometric view of CubeSat; b) structure of solar panel.

through coupling across the gap, excites a fundamental resonant current pattern on the patch (illustrated with solid arrows in Fig. 6.2) in the direction perpendicular to the feed line, indicating a linearly polarized radiation in the far field. This feeding principle also allows multiple patches to be coupled together along the same feed line as long as their central lines are aligned at magnitude maximums of the voltage standing wave.

Changing the solid patch antenna in Fig. 6.2 into a transparent meshed antenna yields Fig. 6.3. The meshed antenna can be made highly transparent (such as 95% transparency) and can be placed on top of solar cells. Such a meshed antenna operating at S band or higher will not affect solar cell's functionality much. In order to promote the desired polarization while suppressing its cross-polarization level, the meshed patch antenna can

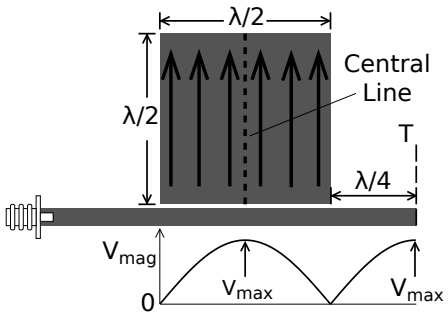

Fig. 6.2: Single patch antenna with proximity feed.

be intentionally designed such that the number of current carrier lines is significantly more than that of equipotential lines. The impedance matching in this design depends primarily on the gap (g in Fig. 6.3) between the patch and the feed line.

6.2.2 Bandwidth Enhancement Mechanism

The proposed method to widen the bandwidth in this paper is achieved by using three meshed patches of slightly different sizes (i.e. three slightly different resonant frequencies), as depicted in Fig. 6.4. The three antennas use the same feed line and such a configuration is highly feasible to be implemented on a multi-U CubeSat (i.e. joining two or three 1U CubeSats together where each 1U CubeSat has a dimension of 10 cm $\times$ 10 cm $\times$ 10 cm) for frequencies higher than S band. The gaps (g_1, g_2, and g_3 in Fig. 6.4) between the meshed patches and the feed line need to be tuned simultaneously in order to achieve a good impedance matching. In addition, it is necessary for all the three patches to generate surface currents in phase, resulting in adding fringing fields. Otherwise, the radiation would be greatly reduced due to sources oscillating in opposite directions. This can be realized when the two adjacent patches are placed on different sides of the feed line.

In the instant the increasing voltage magnitude, as conceptually illustrated in Fig. 6.5 (where the blue arrows indicate the sign of voltage), is formed along the open-ended feed line, decreasing surface currents are induced, via capacitive coupling, flowing in the same direction on both the patches (illustrated with black arrows in Fig. 6.5). The reason for this is that the positive voltage on the feed line pushes "positive charges" on the upper patch away from the gap side while the negative voltage pulls "positive charges" on the

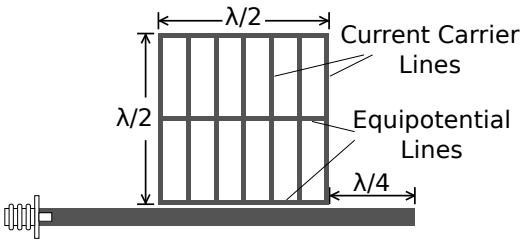

Fig. 6.3: Single meshed patch with proximity feed.

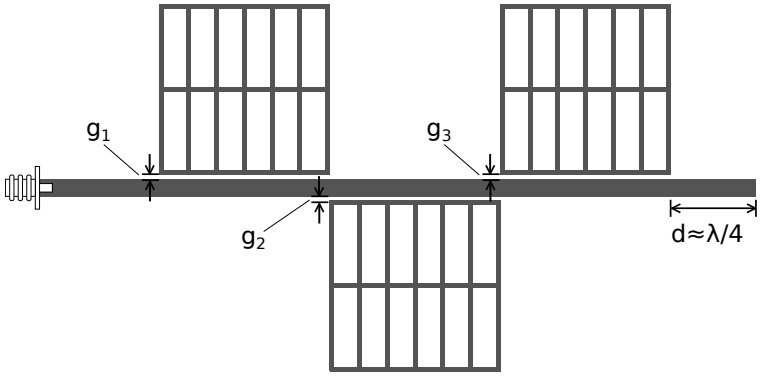

Fig. 6.4: Triple meshed patches with proximity feed.

lower patch towards the gap side. Thus, the two patches resonate with currents adding in phase, leading to constructively polarized radiation in the far field.

The three patch elements in this design may also be placed, with half-wavelength spacing for appropriate phase alignment, on the same side of the feed line, but the proposed configuration shown in Fig. 6.4 ends up being a more compact design, which is suitable for CubeSat applications.

6.3 Results and Discussion

Although in the actual integration with solar cells, a transparent dielectric (e.g. cover glass) will be the substrate for meshed patch antennas, the design philosophy of the CP

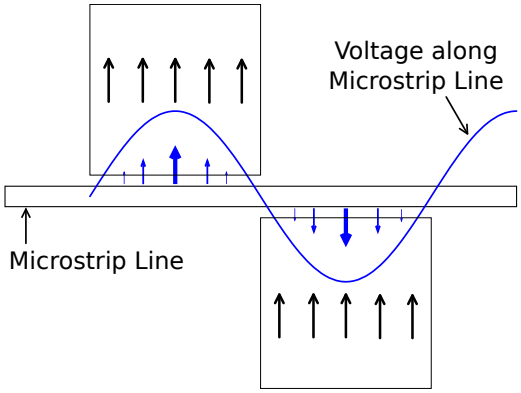

Fig. 6.5: In-phase alignment of patches with proximity feed.

meshed antennas is the same for transparent and non-transparent substrates. Therefore, in the current laboratory validation, Roger's RO4003C laminate (ϵ_r = 3.55, h = 1.524 mm, tanδ = 0.0021) was chosen to examine the design. As a reference antenna, a single-element square patch with 30 mm side length and 1 mm mesh line thickness, as shown in Fig. 6.6, was designed to resonate at about 2.48 GHz and fabricated using a circuit board milling machine. The coupling gap (as g in Figs. 6.3 and 6.4) and the position of the patch with respect to the tip of the feed line were tuned to obtain a good impedance match. Figure 6.7 shows the prototype of the triple-element antenna designed for impedance bandwidth enhancement, where the side lengths of the three patches are 30 mm, 30.2 mm, and 30.4 mm, respectively, while the mesh lines are all of 1 mm width. The transparencies of these patches, defined as the ratio of the area of the openings within the patch to that of the entire patch, are approximately 70%. This transparency is not high enough for the real applications from the solar cells' perspective, however, these parameters were chosen for the ease of fabrication using the milling machine and a very high transparency can be achieved by refining the mesh lines of the patch with a more precise manufacturing facility.

The simulated S_{11} curves of both the single-element and triple-element antennas are plotted in Fig. 6.8, where it can be observed that the 10-dB bandwidth of the triple-element antenna is about 2.5 times as wide as that of the other. The S_{11} values from the

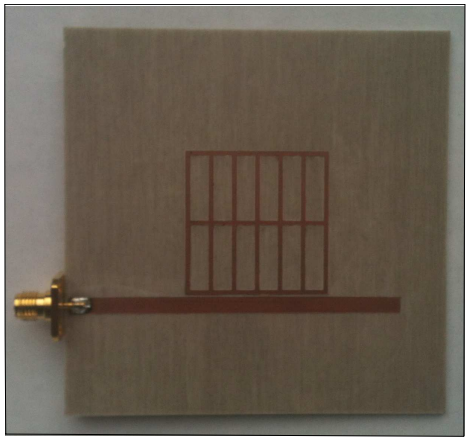

Fig. 6.6: Prototype of single-element meshed antenna.

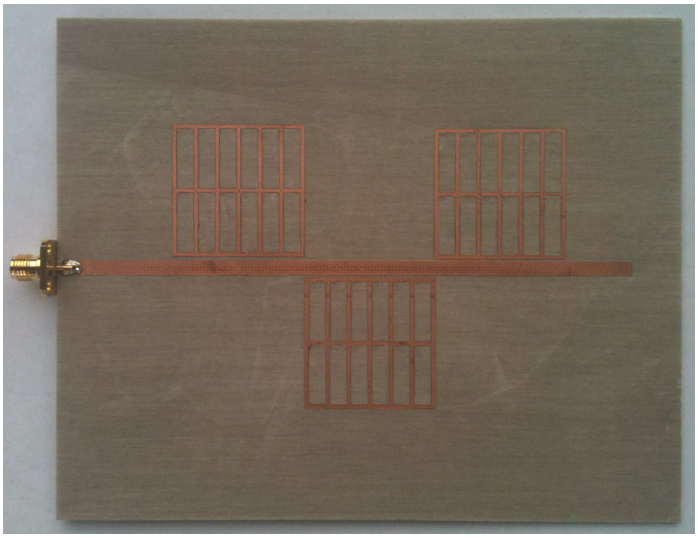

Fig. 6.7: Prototype of proposed meshed antenna.

measurement using an Agilent's VNA 8510C, as in Fig. 6.9, exhibits a very good agreement with the simulation results.

In order to examine other radiation properties of the proposed antenna within the operational frequency band (from 2.413 GHz to 2.478 GHz), its radiation pattern and gain were simulated with Ansys's High Frequency Structure Simulator (HFSS) and measured with the NSI near-field range at three sample frequencies (i.e. 2.43 GHz, 2.45 GHz, and 2.47 GHz). The results are plotted in Figs. 6.10, 6.11, and 6.12, where it can be seen that

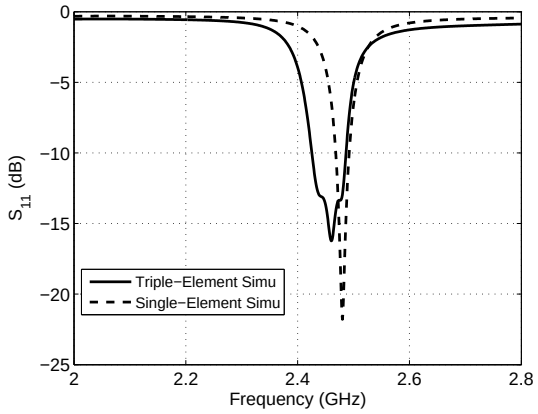

Fig. 6.8: Comparison of simulated S_{11}.

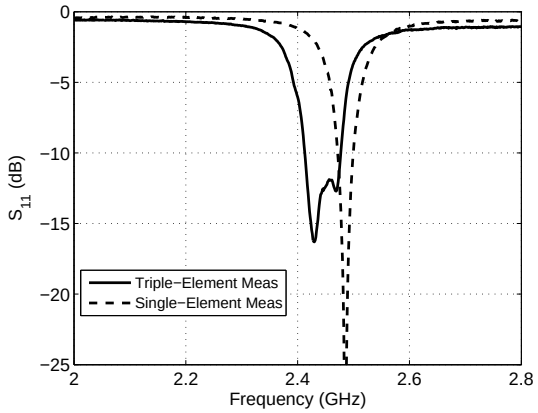

Fig. 6.9: Comparison of measured S_{11}.

the radiation pattern varies with frequency and that the direction of maximum radiation differs. This may be caused by the coupling effects between the closely located patches of the same polarization. The consequence of this is that the antenna may have fluctuated gain in a given direction for different frequencies. The gain measured in the normal direction of the antenna's surface is plotted in Fig. 6.13. Therefore, to increase the bandwidth using this design, the consistency of radiation pattern has to be compromised.

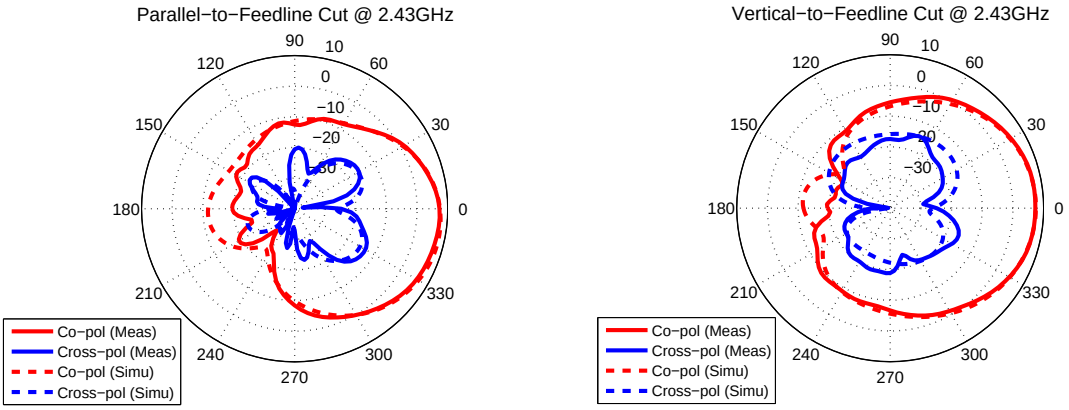

(a) (b)

Fig. 6.10: Radiation pattern of proposed antenna at 2.43 GHz: a) parallel-to-feedline cut; b) vertical-to-feedline cut.

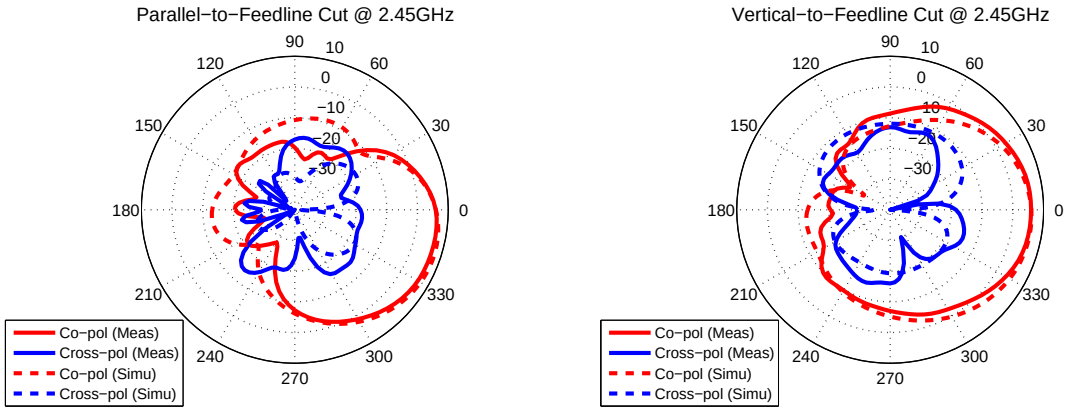

(a) (b)

Fig. 6.11: Radiation pattern of proposed antenna at 2.45 GHz.

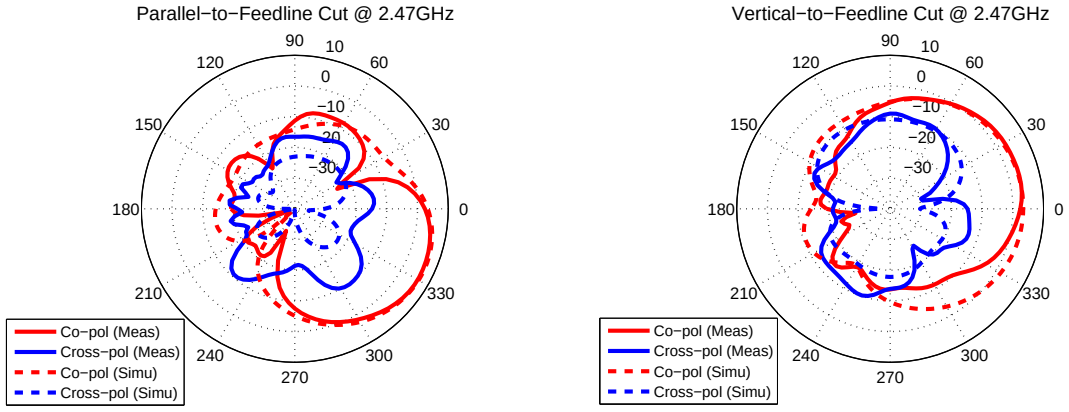

(a) (b)

Fig. 6.12: Radiation pattern of proposed antenna at 2.47 GHz.

6.4 Conclusion

An impedance bandwidth improvement method for optically transparent meshed patch antennas has been presented. The proposed antenna, composed of three meshed patch elements with a common proximity feed line, is highly integratable with solar panels of small satellites and is especially valuable for CubeSats. The results show that the 10-dB bandwidth of the proposed antenna is 2.5 times as wide as that of the single-element meshed patch of the same transparency. Due to the coupling effect between the element patches,

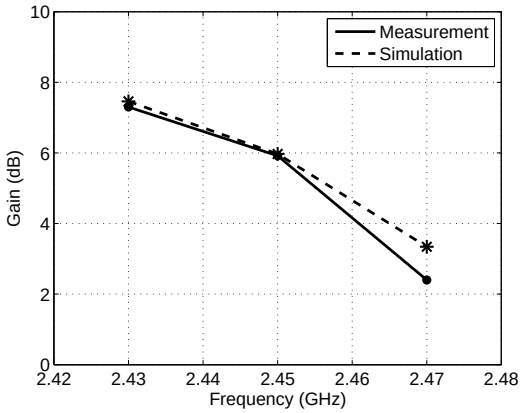

Fig. 6.13: Measured gain variation with frequency in normal direction.

the radiation pattern varies within the operational frequency band. This trade-off can be acceptable in applications where a higher bandwidth is the priority.

References

[1] T. Turpin and R. Baktur, "Meshed patch antennas integrated on solar cells," *IEEE Antennas and Wireless Propagation Letters*, vol. 8, pp. 693–696, 2009.

[2] D. M. Pozar and D. H. Schaubert, *Microstrip Antennas: The Analysis and Design of Microstrip Antennas and Arrays*. New York: IEEE Press, 1995.

[3] H. Pues and A. Van de Capelle, "An impedance-matching technique for increasing the bandwidth of microstrip antennas," *IEEE Transactions on Antennas and Propagation*, vol. 37, no. 11, pp. 1345–1354, 1989.

[4] D. Sun, W. Dou, L. You, X. Yan, and R. Shen, "A broadband proximity-coupled stacked microstrip antenna with cavity-backed configuration," *IEEE Antennas and Wireless Propagation Letters*, vol. 10, pp. 1055–1058, 2011.

[5] S. Hum, J. Chu, R. Johnston, and M. Okoniewski, "Improving the bandwidth of microstrip patch antennas using resistive loading," *IEEE Antennas and Propagation Society International Symposium*, vol. 2, pp. 276–279, 2003.

[6] H. Griguer, E. Marzolf, H. Lalj, F. Riouch, and M. Drissi, "Patch antenna bandwidth enhancement through the use of metamaterials," *International Conference on Telecommunications*, pp. 323–327, 2009.

[7] T. W. Turpin, "Meshed patch antennas integrated on solar cell - a feasibility study and optimization," Master's thesis, Utah State University, Logan, UT, 2009.

[8] T. Miyazaki and K. Itoh, "Analysis and design on a proximity fed microstrip antenna," *Proceedings of the International Symposium on Antennas and Propagation Japan*, vol. 2, pp. 545–548, 1996.

[9] J. Saberin, "Optically transparent antennas for small satelllites," Master's thesis, University of Utah, Logan, UT, 2010.

Chapter 7

Two Types of Optically Transparent Antennas

Abstract

A comparative study on two types of optically transparent antennas is presented. The first type is patch antennas designed from indium tin oxides (ITO) films. It is shown that such an antenna has no more than 20% efficiency at S band when the optical transparency needs to be 90% or higher. The low efficiency is mainly limited by today's material processing technology. At frequencies higher than Ku band, however, ITO patch antennas are effective radiators. Meshed patch antennas are the second type of transparent antennas, and it is shown that a meshed antenna can be optimized simultaneously for both optical transparency and antenna efficiency. Meshed patch antennas have the most advantages at frequency bands lower than 5 GHz but are difficult to prototype when the operational frequency is higher. The paper also shows that it is feasible to improve the efficiency of an ITO antenna by combining metal lines with the ITO film on the patch geometry.

7.1 Introduction

Optically transparent antennas have been drawing increased interest since this concept was introduced [1–20]. One straightforward method to design such antennas is to use transparent conductors such as AgHT-8 and transparent conductive oxides (TCO). Among TCO films, indium tin oxides (ITO) films have become a preferred material because of their reasonable trade-off between optical transparency and conductivity. Another method to design an optically transparent antenna is to use meshed conductors [4–7].

It is found that most reported development of ITO antennas is of monopole geometry [18–20], whereas not much has been done for patch antennas. Transparent patch antennas are important in applications where being conformal to the mounting surface is essential. A

typical application can be integration of a transparent antenna with the solar cells of small satellites [7]. Saberin performed a study on ITO patch antennas and analyzed antenna efficiency on a glass substrate [21]. As the dielectric constant of the glass is fairly high for an effective antenna design, it is necessary to perform a more detailed study by considering different substrates. In addition, most ITO antennas have a transparency of less than 80% [21], which is not sufficient for applications where a higher transparency such as 90% is needed. On the other hand, it is very convenient to design a highly transparent meshed patch antenna, especially in the lower GHz range.

This paper aims to present the properties of and design methods for highly transparent (90% transparency or higher) patch antennas designed from ITO and meshed conductors. Another objective of this paper is to provide a comparison on the two types of transparent patch antennas in terms of transparencies, efficiency, and operational frequencies.

7.2 ITO Patch Antennas

In this section, if not specified particularly, all the ITO patch antennas were designed to have an ITO film patch (45 mm $\times$ 37 mm) on top of the same substrate ($\epsilon_r = 2$, $tan\delta = 0.0057$, $h = 2$ mm) backed with copper ground plane. Such geometry has been chosen mainly based on the small satellite application, where the transparent antennas are to be integrated on top of the solar cells and the ground plane is the metal surface of the satellite. Therefore, the ground does not have to be transparent. The effect of solar cells on the antenna performance is not the objective of this paper as the main goal is to show the antenna design matrix. All the simulations have been studied using Ansys's High Frequency Structure Simulator (HFSS). And the ground plane (i.e. the size of the substrate) was set to be large enough (105 mm $\times$ 105 mm) so that the antenna properties such as gain and efficiency would become independent of the ground plane size, when operating at S band and above.

7.2.1 Basic Properties of ITO Films

Efficiency of a patch antenna is primarily determined by the conductivity of the patch

material. Therefore, it is important to assess the material parameters that affect the conductivity and transparency of an ITO film. ITO is indium oxide doped with tin oxide. The electrical conductivity and optical transparency of an ITO film are highly dependent on the material properties, which are mostly decided during doping and deposition process. It is found that high conductivity is balanced against high transparency in the visible spectrum [21–23].

For an ITO film to be considered as a conductor, the operational frequency has to be below the plasma frequency of the film [21–23]. The plasma frequency, which is also a limiting factor for optical transparency, is determined from free electron density N_e of ITO, electron charge q, effective mass of an electron m^*, and electron relaxation/scattering time τ [21–23]. For an ITO film to be transparent in visible spectrum and conductive in microwave band, the plasma frequency needs to be carefully designed. The optical transparency, or the transmission coefficient $T(t)$, of the ITO film can be approximated by (7.1), where t is the film thickness, and δ_l is the skin depth for visible light [22]. The skin depth δ_l can be obtained using (7.2), where Z_∞ is equal to $377/\epsilon_\infty^{1/2}$, and ω_l is the frequency of visible light [23].

$$T(t) \approx e^{2t/\delta_l} \tag{7.1}$$

$$\delta_l \approx \frac{2m^*\omega_l^2\tau}{Z_\infty q^2 N_e} \tag{7.2}$$

From (7.1) and (7.2), it is obvious that a higher transparency requires a thinner film with a higher skin depth at visible light frequencies.

The electrical conductivity can be derived from the surface resistance of an ITO film. The surface resistance is computed from

$$R_s = 1/(N_e q \mu_e t), \tag{7.3}$$

where μ_e is the electron mobility [21–23]. At a microwave frequency ω, the electrical conductivity is related to the microwave skin depth δ_m, which can be approximated from

$$\delta_m \approx \sqrt{2/(\omega\mu\sigma)}. \tag{7.4}$$

For a higher conductivity, a thicker film with higher N_e and μ_e is needed. In addition, it is straightforward to see that the thickness of the film t needs to be much higher than the skin depth δ_m at the given antenna operational frequencies. To maximize both optical transparency and electrical conductivity, N_e can only be at its maximum 1.5×10^{21} cm^{-3} [21–23], and μ_e should be as high as possible. According to the literature [22,23], high quality ITO films with μ_e up to 50 $\text{cm}^2\text{V}^{-1}\text{s}^{-1}$ are available from the current material technology.

7.2.2 Analysis and Discussions

Effect of Electron Mobility

Since the electron mobility μ_e of an ITO film is the only variable of material parameters that can affect both transparency and conductivity in the same manner, it is reasonable to expect that a higher μ_e value produces an ITO film with better electrical and optical quality.

Using (7.1) and (7.2), and the relationship between μ_e and τ [23], the relation between the electron mobility, thickness of the ITO film, and the optical transparency were computed. The results are presented in Fig. 7.1. The surface resistance of the ITO film for varied electron mobility and optical transparency was computed from (7.3) and plotted in Fig. 7.2. It is clear from Fig. 7.1 and Fig. 7.2 that at a given transparency, a higher electron mobility allows for a higher thickness of the ITO film, which helps reduce the surface resistance and hence the loss.

To examine how the electron mobility μ_e affects the antenna's radiation efficiency, three sets of patch antennas with different transparencies were studied using HFSS. The operation frequency of these antennas was about 2.5 GHz. The thickness of the ITO film

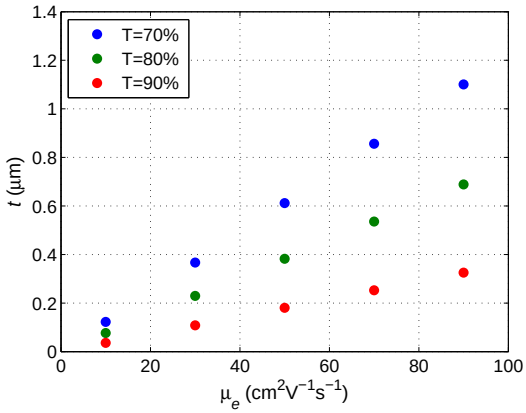

Fig. 7.1: Thickness vs. electron mobility.

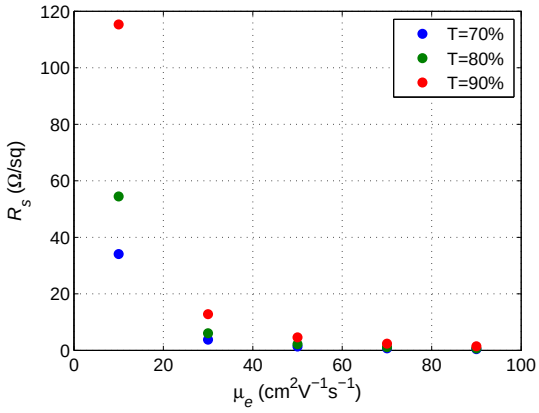

Fig. 7.2: Surface resistance vs. electron mobility.

was extracted from Fig. 7.1. The results are plotted in Fig. 7.3. As expected, a higher electron mobility results in a higher antenna efficiency. Also, for the same electron mobility, a higher transparency implies a lower efficiency. The current material development shows that the maximum mobility is about 50 $cm^2V^{-1}s^{-1}$, and therefore Fig. 7.3 indicates that a 90% transparent antenna has an efficiency of less than 15% at about 2.5 GHz.

Effect of Operational Frequency

For given electron mobility and transparency, the surface resistance and the thickness of the film are fixed. But since the skin depth of the ITO film depends on antenna's operational frequency according to (7.4), it is expected that a higher frequency predicts a lower skin

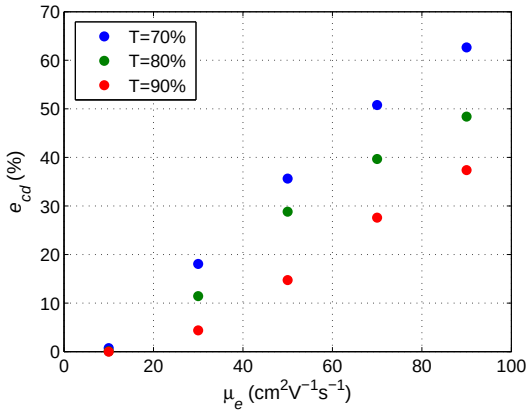

Fig. 7.3: Effect of electron mobility on antenna's radiation efficiency.

depth, and hence a more efficient antenna. A group of five patch antennas designed from the same ITO film of current technology, but at five different resonance frequencies, were examined. The transparency was set to be 80%. The computed efficiency is presented in Fig. 7.4. It is seen that at about 5 GHz, an 80% transparent ITO patch antenna has about 50% efficiency.

For integration with solar cells, an antenna needs to have at least 90% transparency. Therefore, a 90% transparent ITO patch antenna at 5 GHz was studied. And its efficiency is found to be about 32% for the same substrate as in the previous two studies. Although

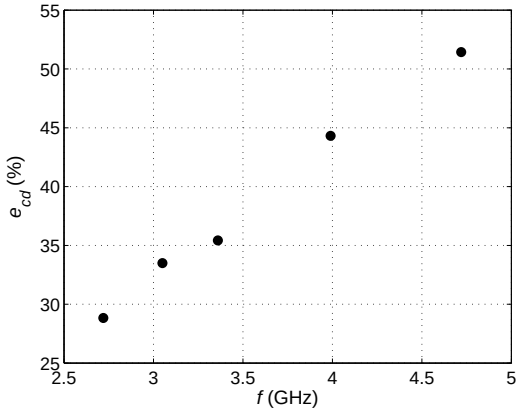

Fig. 7.4: Radiation efficiency vs. resonance frequency.

this efficiency is still low, it indicates a feasible gain of 3 dB and possibility of an integrated solar panel array antenna design to achieve a higher gain for practical satellite missions.

Effect of Dielectric Constant of the Substrate

It is known that a substrate with a lower permittivity leads to a patch antenna with a higher gain. To see the maximum possible efficiency of an 80% transparent ITO (of current technology) patch antenna at about 2.5 GHz, the antenna efficiency for varied substrate permittivity was evaluated. The thickness and tangential loss of the substrate were remained unchanged. The results are plotted in Fig. 7.5, where it can be seen that the efficiency of an 80% transparent antenna is less than 45% for a permittivity smaller than 2.

7.3 Meshed Patch Antennas

Transparent antennas can be designed from meshed conductors [1, 2], where the openings in the meshed metal screen allow light to go through and yet the sheet can still be an effective radiator at microwave frequencies. Compared to ITO antennas, meshed antennas are less expensive and readily available as one can either get meshed conductors off the shelf or create a mesh geometry using a printing technique such as screen printing [7, 24] or an inkjet printing [25]. Clasen and Langley studied meshed patch antennas and showed

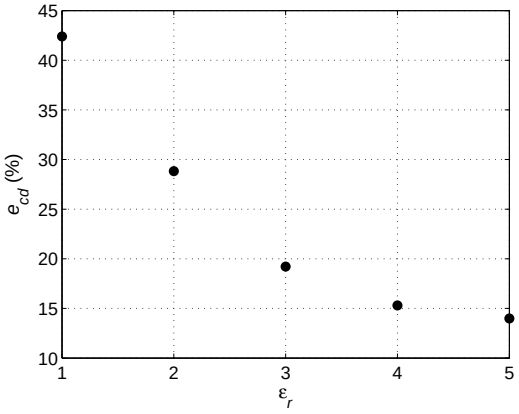

Fig. 7.5: Radiation efficiency vs. dielectric constant.

that a more transparent mesh produces a less effective antenna [4]. It is found that Clasen and Langley reached such a conclusion by varying mesh transparency through changing the number of mesh lines while fixing the mesh linewidth. This section presents a more detailed examination on how mesh geometry affects the antenna performance.

7.3.1 Optimal Design for Transparent Meshed Patch Antennas

Meshed patch antennas, compared to their solid counterparts, have higher surface resistance due to much less conductor coverage. Therefore, it is normal to have degraded antenna performance for increased optical transparency [4]. This statement, however, is found not exclusive. Turpin has shown that for a rectangular meshed patch antenna, the efficiency of the antenna can be improved to be comparable to that of a solid patch by refining the width of the mesh line [24].

For a comparison, three sets of rectangular meshed patch antennas with different transparencies (70%, 80%, and 90%) were designed on the same substrate as in the previous section and studied with HFSS. For each of them, copper was used for both the meshed patch and the solid ground plane. The thickness of copper was taken at least 20 times of the skin depth. The geometry of the rectangular meshed patch antenna is shown in Fig. 7.6. The transparency of the patch is defined as the ratio of the area of the see-through parts (i.e. the area of the patch minus the total metal area) to the total area of the patch.

For each transparency, one can achieve the transparency by varying the linewidth and number of mesh lines. The efficiency of the meshed antenna as a function of the linewidth

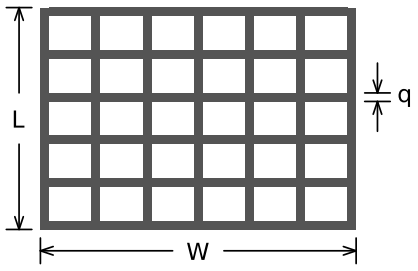

Fig. 7.6: Geometry of rectangular meshed patch.

for each transparency is plotted in Figs. 7.7, 7.8, and 7.9. It is clear that for a given transparency, the efficiency of a meshed antenna can be improved by refining the linewidth. From fabrication standpoint, achieving a linewidth of 0.1 mm or wider is not challenging in practice. From Fig. 7.9, it is seen that with a linewidth of 0.1 mm, it is feasible to achieve an efficiency of more than 60% for an antenna of 90% transparency. Such efficiency and transparency are adequate for solar cell integration and a nano-satellite's communication needs.

It is further found that only the mesh lines in the direction of the current flow of the resonant mode (i.e. the mesh lines along L in Fig. 7.6) have major effect on the antenna

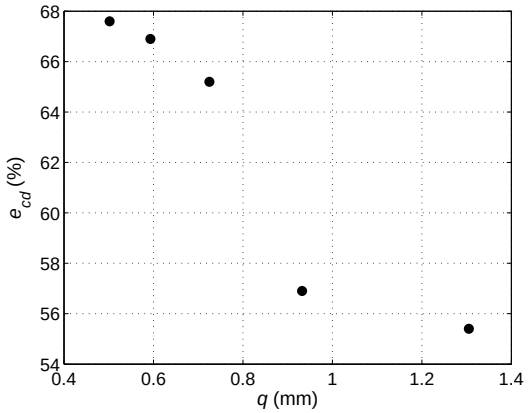

Fig. 7.7: Radiation efficiency vs. mesh linewidth (70%).

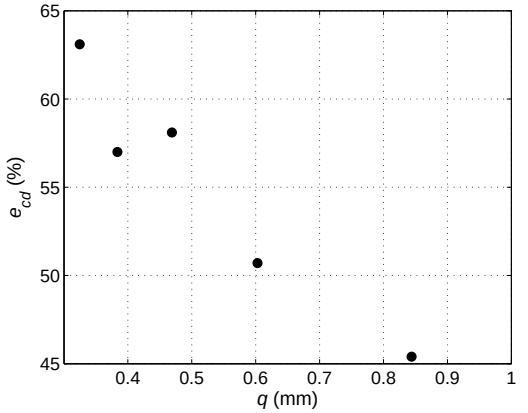

Fig. 7.8: Radiation efficiency vs. mesh linewidth (80%).

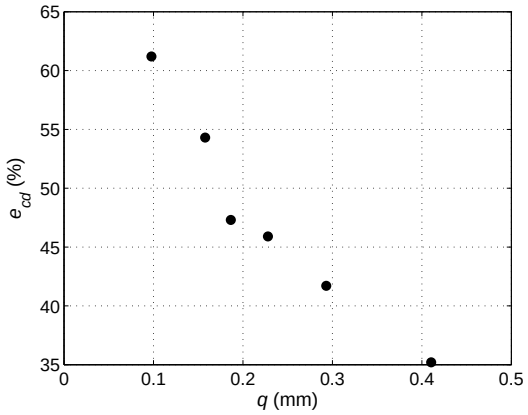

Fig. 7.9: Radiation efficiency vs. mesh linewidth (90%).

performance [24]. Therefore, the transparency of a meshed patch antenna can be further improved by reducing lines that are parallel to W (Fig. 7.6) to the minimum.

7.3.2 Gain Reduction Due to Meshing

Using the optimization method discussed in Section 7.3.1, four meshed copper antennas with the same patch size but different transparencies were designed on the substrate (ϵ_r = 2.6, $tan\delta$ = 0.002, h = 2.032 mm) backed with solid copper ground plane and were compared against their solid patch counterpart. The purpose of this study was to examine how the meshing affects the gain of copper patch antennas. The simulation results are listed in Table 7.1, where it can be seen that the gain loss of the antenna due to meshing is close to 2.5 dB for the 95% transparent meshed patch and that such loss decreases with reduced transparency. Therefore, it can be concluded that even when a meshed antenna is optimized by refining the lines, the antenna suffers a gain loss due to the act of meshing. Such a gain reduction is higher for a meshed antenna with a higher transparency.

7.3.3 Comparison of Meshed Patches and ITO Patches

The two types of transparent antennas with 90% transparency were compared to provide a reference in choosing appropriate antenna solutions for different applications. As has been discussed in Section 7.2, the radiation efficiency of 90% transparent ITO antennas

Table 7.1: Meshing effect on the gain of rectangular meshed copper patch (45 mm × 37 mm).

$G_{0,solid}$ (dB)	7.32			
Mesh Trans. (%)	70	80	90	95
$G_{0,meshed}$ (dB)	6.52	6.08	5.25	4.90
$G_{0,meshed}$ - $G_{0,solid}$ (dB)	-0.80	-1.24	-2.07	-2.42

is as low as no more than 15%. However, it is not challenging to achieve a meshed patch antenna with a reasonable efficiency ($\geqslant$ 50%) as well as a high optical transparency ($\geqslant$ 90%), as shown in Fig. 7.9. Therefore, meshed patch antennas are more advantageous for low frequency (e.g. S-band) applications.

In order to investigate higher frequency (from 5 GHz to 20 GHz) behavior, four ITO (of current technology) patch antennas of 90% transparency designed on the same substrate were studied. The results are listed in Table 7.2, where it can be observed that the antenna's gain and efficiency are improved with the increased frequency. The reason for this is that the thickness of the 90% transparent ITO film becomes "thicker" at a higher frequency in terms of skin depth. On the other hand, the fabrication of meshed antennas becomes more challenging at higher frequencies as the size of the antenna becomes smaller and the linewidth becomes very thin in order to keep up the high transparency (Table 7.3). Thus, ITO antennas are more suitable for high frequency applications compared to the meshed ones.

In addition, for applications where one needs the antenna to be "invisible," the ITO antenna may become the only solution and one has to sacrifice transparency to yield an applicable gain.

Table 7.2: Frequency study on 90% transparent ITO patch antenna.

Freq (GHz)	5.4	11.0	15.6	20.2
S_{11} (dB)	-18.8	-43.6	-25.1	-45.3
Gain (dB)	1.3	4.0	6.4	6.7
Efficiency (%)	21.1	37.4	65.9	75.2

Table 7.3: Geometry of 90% transparent meshed patch antenna with seven horizontal and seven vertical lines.

Freq (GHz)	5.4	11.0	15.6	20.2
Patch Size (mm^2)	22.0 × 17.7	11.0 × 8.6	7.3 × 5.5	5.5 × 3.9
Linewidth (mm)	0.14	0.069	0.045	0.033

7.4 Antennas Designed from AgHT

Silver coated polyester (AgHT) films have also been used for transparent antenna application [8]. In general, the transparency of AgHT films is lower than 70% for an effective conductivity. Surface resistance of two typical AgHT films is listed in Table 7.4. It is seen that an AgHT film of 75% transparency has a similar surface resistance as a 90% transparent ITO film. This means the efficiency of the antenna will be lower than 20% at about 2.5 GHz. Therefore, in order to design an effective antenna from AgHT films, the transparency has to be remained very low.

7.5 Combo-Material Design

It has been shown that the efficiency of an ITO antenna can be improved by applying narrow strips of highly conductive coating (e.g. copper) on specific areas of the antenna [8]. Normally, the selected area should be where highest current density is. For a rectangular patch antenna, the areas that have relatively higher current density are the non-radiating side edges of the patch. In this study, a rectangular patch antenna designed from the 90% transparent ITO film (of current technology) combined with copper edgings is discussed. The antenna geometry is shown in Fig. 7.10, where the width of the copper strips are 0.5 mm. The simulation result shows that the antenna efficiency is improved to 29% as opposed to 15% efficiency of the same antenna without edgings (Fig. 7.3). However, the overall transparency has to be sacrificed since the copper is non-transparent.

Table 7.4: Surface resistance comparison.

Material	90% ITO Film	75% AgHT-4 Film	82% AgHT-8 Film
Surface Resistance (Ω/sq)	4.6	4.5	8

Fig. 7.10: Patch antenna made from ITO film (90% transparency) with parallel copper edges.

7.6 Conclusion

Optically transparent antennas can be designed from transparent conductors or from meshed conductors. Among transparent conductors, ITO films have higher transparency for an acceptable conductivity. As to an ITO patch antenna, it is seen that for a given transparency, the efficiency of the antenna is mainly determined by the electron mobility and operational frequency. While the electron mobility is limited by today's available material processing technology, one may achieve an efficient ITO antenna at a frequency higher than 10 GHz if one desires an optical transparency of 80% or higher. In addition, choosing a substrate with a lower dielectric constant is another known method to improve the antenna's gain to certain extent. Meshed patch antennas can be designed to have a high transparency while maintaining good efficiency. But meshed antennas become challenging to fabricate for frequencies higher than 10 GHz. Therefore, for applications where a high transparency is desired, the meshed antenna is a more effective solution for lower GHz bands, and ITO films have more advantages for frequencies higher than Ku bands. In addition, it is possible to improve the gain of an ITO patch antenna by combining metal coating with the ITO film. But one should consider the trade-offs between the improvement and the "invisibility" as metal coatings are not transparent.

References

[1] G. Andrasic and J. James, "Microstrip window array," *Electronics Letters*, vol. 24, no. 2, pp. 96–97, 1988.

[2] K. Ito and M. Wu, "See-through microstrip antennas constructed on a transparent substrate," *ICAP 91, Seventh International Conference on (IEE) Antennas and Propagation*, pp. 133–136 vol.1, 1991.

[3] R. N. Simons and R. Q. Lee, "Feasibility study of optically transparent microstrip patch antenna," *IEEE Antennas and Propagation Society International Symposium*, vol. 4, pp. 2100–2103, 1997.

[4] G. Clasen and R. J. Langley, "Meshed patch antennas," *IEEE Transactions on Antennas and Propagation*, vol. 52, no. 6, pp. 1412–1416, 2004.

[5] ——, "Meshed patch antenna integrated into car windscreen," *Electronics Letters*, vol. 36, no. 9, pp. 781–782, 2000.

[6] ——, "Gridded circular patch antennas," *Microwave and Optical Technology Letters*, vol. 21, no. 5, pp. 311–313, 1999.

[7] T. Turpin and R. Baktur, "Meshed patch antennas integrated on solar cells," *IEEE Antennas and Wireless Propagation Letters*, vol. 8, pp. 693–696, 2009.

[8] H. J. Song, T. Y. Hsu, D. F. Sievenpiper, H. P. Hsu, J. Schaffner, and E. Yasan, "A method for improving the efficiency of transparent film antennas," *IEEE Antennas and Wireless Propagation Letters*, vol. 7, pp. 753–756, 2008.

[9] T. Peter, T. Yuk, R. Nilavalan, and S. Cheung, "A novel technique to improve gain in transparent UWB antennas," *Loughborough Antennas and Propagation Conference (LAPC)*, pp. 1–4, 2011.

[10] T. Peter, R. Nilavalan, H. Abu Tarboush, and S. Cheung, "A novel technique and soldering method to improve performance of transparent polymer antennas," *IEEE Antennas and Wireless Propagation Letters*, vol. 9, pp. 918–921, 2010.

[11] O. Yurduseven, D. Smith, N. Pearsall, and I. Forbes, "A transparent solar patch antenna for 2.4/2.5 GHz WLAN-WiMAX applications," *2012 2nd International Symposium on Environment Friendly Energies and Applications (EFEA)*, pp. 614–617, 2012.

[12] M. J. Roo-Ons, S. V. Shynu, M. Ammann, S. McCormack, and B. Norton, "Transparent patch antenna on a-Si thin-film glass solar module," *Electronics Letters*, vol. 47, no. 2, pp. 85–86, 2011.

[13] N. Guan, H. Furuya, K. Himeno, K. Goto, and K. Ito, "A monopole antenna made of a transparent conductive film," *IWAT '07 International Workshop on Antenna Technology: Small and Smart Antennas Metamaterials and Applications*, pp. 263–266, 2007.

[14] A. Katsounaros, Y. Hao, N. Collings, and W. Crossland, "Optically transparent antenna for ultra wide-band applications," *EuCAP 2009. 3rd European Conference on Antennas and Propagation*, pp. 1918–1921, 2009.

[15] N. Guan, H. Furuya, R. Hosono, H. Tayama, and K. Yamagami, "A see-through wire-grid film antenna for WLAN applications," *IEEE Asia-Pacific Conference on Antennas and Propagation (APCAP)*, pp. 273–274, 2012.

[16] J. Hautcoeur, F. Colombel, X. Castel, M. Himdi, and E. Cruz, "Optically transparent monopole antenna with high radiation efficiency manufactured with silver grid layer (AgGL)," *Electronics Letters*, vol. 45, no. 20, pp. 1014–1016, 2009.

[17] C. Mias, C. Tsakonas, N. Prountzos, D. C. Koutsogeorgis, S. C. Liew, C. Oswald, R. Ranson, W. Cranton, and C. Thomas, "Optically transparent microstrip antennas," *IEE Colloquium on Antennas for Automotives (Ref. No. 2000/002)*, pp. 8/1–8/6, 2000.

[18] C.-T. Lee, C.-M. Lee, and C.-H. Luo, "The transparent monopole antenna for WCDMA and WLAN," *IEEE Annual Wireless and Microwave Technology Conference*, pp. 1–3, 2006.

[19] F. Colombel, X. Castel, M. Himdi, G. Legeay, S. Vigneron, and E. M. Cruz, "Ultrathin metal layer, ITO film and ITO/Cu/ITO multilayer towards transparent antenna," *IET Science, Measurement & Technology*, vol. 3, no. 3, pp. 229–234, 2009.

[20] N. Guan, H. Furuya, D. Delaune, and K. Ito, "Radiation efficiency of monopole antenna made of a transparent conductive film," *IEEE Antennas and Propagation Society International Symposium*, pp. 221–224, 2007.

[21] J. Saberin, "Optically transparent antennas for small satelllites," Master's thesis, University of Utah, Salt Lake City, UT, 2010.

[22] P. P. Edwards, A. Porch, M. O. Jones, D. V. Morgan, and R. M. Perks, "Basic materials physics of transparent conducting oxides," *Dalton Transactions*, no. 19, pp. 2995–3002, 2004.

[23] A. Porch, D. V. Morgan, R. M. Perks, M. O. Jones, and P. P. Edwards, "Electromagnetic absorption in transparent conducting films," *Journal of Applied Physics*, vol. 95, no. 9, pp. 4734–4737, 2004.

[24] T. W. Turpin, "Meshed patch antennas integrated on solar cell - a feasibility study and optimization," Master's thesis, Utah State University, Logan, UT, 2009.

[25] J. A. Arellano, "Inkjet-printed highly transparent solar cell antennas," Master's thesis, Utah State University, Logan, UT, 2011.

Chapter 8

Conclusion

8.1 Summary

Transparent patch antennas designed from different materials using different approaches have been presented in this dissertation. Particularly, an optimization method for both transparency and efficiency, harmonic suppression feature for active integrated antenna (AIA) applications, coplanar antenna designs for circular polarization (CP), and a technique for bandwidth improvement have been developed for meshed patch antennas. Moreover, properties of transparent patch antennas made from transparent conductive oxides (TCO) films have been discussed.

For the most part of this dissertation, transparent meshed patches for small satellite applications have been studied. Antenna prototypes have been fabricated and measured. It is demonstrated that the proposed meshed patch antennas possess compatible structures for integration with solar cells. Chapter 2 discussed an optimization method to fully explore meshed antennas' potential without comprising either radiation efficiency or optical transparency. Circular meshed patch antennas with harmonics-tuning functionality was described in Chapter 3. In practice, such antennas can improve the amplifier's power efficiency, reduce electromagnetic interference (EMI) due to radiation at higher harmonics and thus harmonics-tuning filters are not required any more in the front end subsystem, which facilitates a compact system design. Chapter 4 and 5 presented two different meshed patch antenna designs for CP and it is of significance, especially for geo-satellite communications. The multiple-resonance bandwidth improvement approach was applied to design a meshed patch antenna with increased bandwidth in Chapter 6.

In Chapter 7, transparent patch antennas made from indium tin oxides (ITO) films were analyzed and then compared against meshed patches in terms of optical transparency

and radiation efficiency. It is found that ITO patch antennas are more suitable for higher frequency applications (e.g. array application at K- or Ku-band).

Overall, it is promising to employ the proposed antennas to small satellites, especially smaller ones such as CubeSats, and to carry out a customized design to meet different requirements.

8.2 Future Work

The research presented in this dissertation may be extended in several ways. The ultimate goal of this research is to promote practical application of transparent patch antennas to small satellites. Therefore, more knowledge is needed about the antenna performance with the presence of real working solar cells in space environment. This can be the first extension to the work accomplished in this dissertation. Also, it is very critical for the meshed patch antennas to become commercialized. Although satellite solar panel structures are considered and maximum transparency is attainable in each design given in this dissertation, practical questions about the changes in material properties in space environment and about comprehensive evaluation of both antenna performance and solar cell functionality are not yet addressed.

Some other extensions may be made in array applications of transparent patch antennas. As discussed in Chapter 7, regular meshed patches are favored at lower frequencies (e.g. S-band) whereas ITO patch antennas perform better at higher frequencies such as in K- or Ku-band. Following this conclusion, different antenna arrays can be designed at different frequency bands to improve antenna properties or to control the radiation patterns electronically. These applications can be used on larger small satellites where required surface space is available.

Vita

Tursunjan Yasin

Education

Ph.D in Electrical Engineering, Utah State University, Logan, Utah (2008 $\sim$ 2013)

M.S. in Electronic Engineering, Tsinghua University, Beijing, China (2001 $\sim$ 2004)

B.S. in Electronic Engineering, Tsinghua University, Beijing, China (1997 $\sim$ 2001)

Journal Papers

- Active Integrated Meshed Patch Antennas for Small Satellites, Alper Genc, Tim Turpin, Tursunjan Yasin, Reyhan Baktur, *Microwave and Optical Technology Letters*, vol. 54, pp. 1593-1595, 2012.
- Circular Meshed Patch Antenna with Harmonic Suppression Functionality for Integration with Power Amplifiers, Tursunjan Yasin and Reyhan Baktur, *to be submitted.*
- Circularly Polarized Meshed Patch Antenna for Small Satellite Application, Tursunjan Yasin and Reyhan Baktur, *to be submitted.*
- Bandwidth-Enhanced Meshed Patch Antenna Design, Tursunjan Yasin and Reyhan Baktur, *to be submitted.*
- Circularly Polarized Meshed Patch Antenna Using Coplanar Y-Shaped Coupling Feed, Tursunjan Yasin and Reyhan Baktur, *to be submitted.*
- Optimized Design Method for Highly Transparent Meshed Patch Antennas, Timothy W. Turpin, Tursunjan Yasin and Reyhan Baktur, *to be submitted.*
- Two Types of Optically Transparent Antennas, Tursunjan Yasin and Reyhan Baktur, *to be submitted.*

Conference Papers

- Optically Transparent Multifunctional Patch Antennas Integrated with Solar Cells for Small Satellites, Tursunjan Yasin and Reyhan Baktur, in *25th Annual AIAA/USU Conference on Small Satellites*, Aug 2011.

- A Study on the Efficiency of Transparent Patch Antennas Designed from Conductive Oxide Films, Tursunjan Yasin and Reyhan Baktur, in *Proceedings of IEEE International Symposium on Antennas and Propagation*, July 2011.

- A Comparative Study on Two Types of Transparent Patch Antennas, Tursunjan Yasin and Reyhan Baktur, in *URSI General Assembly*, Aug 2011.

- Inkjet-Printed Patch Antennas on Transparent Substrates, Tursunjan Yasin and Reyhan Baktur, in *Proceedings of IEEE International Symposium on Antennas and Propagation*, Aug 2010.

- Inkjet-Printed Transparent Antennas Integrated on Solar Cells, Tursunjan Yasin, Reyhan Baktur, Jason Saberin, Cynthia Furse, in *24th Annual AIAA/USU Conference on Small Satellites*, Aug, 2010.

- Passive Feed Methods for Meshed Antennas, Jason R. Saberin, Cynthia Furse, Tursunjan Yasin and Reyhan Baktur, in *Proceedings of IEEE International Symposium on Antennas and Propagation*, Spain, July, 2010.